Lithos 342–343 (2019) 1–17

Contents lists available at ScienceDirect

Lithos

journal homepage: www.elsevier.com/locate/lithos

Tracing the history from Rodinia break-up to the Gondwana amalgamation in the Embu Terrane, southern Ribeira Belt, Brazil

Cláudia R. Passarelli [a,*], Sanjeet K. Verma [b], Ian McReath [a], Miguel A.S. Basei [a], Oswaldo Siga Jr [a]

[a] Instituto de Geociências, Universidade de São Paulo, Rua do Lago 562, Cidade Universitária, São Paulo, SP CEP 05508-080, Brazil
[b] División de Geociencias Aplicadas, Instituto Potosino de Investigación Científica y Tecnológica, Col. Lomas 4ª Sec, San Luis Potosí C.P. 78216, Mexico

ARTICLE INFO

Article history:
Received 16 March 2019
Accepted 17 May 2019
Available online 23 May 2019

Keywords:
West Gondwana, Ribeira Belt-Embu Terrane
LA-ICP-MS U–Pb
Lu-Hf isotopes
Granite tectonic setting

ABSTRACT

The Mantiqueira Province (MP) is the major tectonic unit of southern Brazil, resulting from the closure of the Adamastor Ocean during Gondwana assembly. The Ribeira Belt (RB), the largest domain of the MP, has developed in several episodes of convergence during the Brasiliano-Pananafricano Orogeny and is subdivided into several terranes. One of them is the Embu Terrane (ET) that hosts metasedimentary successions and granitic bodies of different tectonic contexts. A combined study of petrography, geochemistry, LA–ICP–MS zircon U—Pb dating, and Hf isotope geology was carried out on the Juquiá (JG) and Sete Barras (SBG) granites of the southeastern ET, hosted by metasupracrustal rocks. The JG yielded U—Pb zircon ages of 799 ± 5 Ma and 755 ± 3 Ma, while the SBG U—Pb zircon and monazite ages of 602 ± 2 Ma and 598 ± 2 Ma respectively. Both granites have Neoarchean/Paleoproterozoic Hf (T_{DM}) model ages and strongly negative $\varepsilon Hf_{(t)}$ values in zircon. Whole rock isotopic data support an evolved crustal signature, pointing to sources of long-lived crustal residence. The JG is a ferroan calc-alkalic peraluminous two-mica granite, while the SBG is a ferroan alkali-calcic peraluminous two-mica granite. The acquired data disclose two distinct magmatic episodes in ET: the Tonian Juquiá magmatism took place during the final stages of the Rodinia break-up or initial stages of expansion of one of the hypothetical oceans in the region and the Ediacaran Sete Barras magmatism might have been formed at the local transtensional area during final West Gondwana amalgamation. The data presented here and the wide-ranging geochronological data assemblage from the RB allowed a new paleogeographic reconstruction of the West Gondwana assembly.

1. Introduction

The Mantiqueira Province (MP) is mainly composed of the Dom Feliciano, Ribeira and Araçuaí orogenic belts, whose segments encompass a large number of tectonic and regional denominations (Almeida et al., 2000; Basei et al., 2010; Silva et al., 2005). The largest geotectonic unit of the MP is the Ribeira Belt (RB) (Heilbron et al., 2004a; Silva et al., 2005), which formed by the closure of the Adamastor Ocean due to the interaction between the São Francisco, Paranapanema, Rio de la Plata, Luis Alves, Congo and Kalahari cratons during Gondwana assembly (Fig. 1a). The Embu Terrane (ET) is part of the RB and is composed of predominantly metasupracrustal sequences affected by medium to high-grade metamorphism, Paleoproterozoic basement and successive Neoproterozoic periods of granite magmatism with typically crustal signatures since the Tonian (Alves et al., 2016).

Although recent geochronological studies have been performed on the understanding on granitic magmatism and the depositional ages of the metavolcanosedimentary sequences in this domain (Campanha et al., 2019; Costa et al., 2017; Duffles et al., 2016), its tectonic significance within the RB is still unclear. Petrographic and geochronological studies were carried out on several peraluminous granites intrusive into the metasupracrustal sequences and the deformed Tonian granites are interpreted as record of an early episode of plate convergence (Vlach, 2001; Cordani et al., 2002; Alves et al., 2013, reference therein) and within-plate divergent processes (Campos Neto et al., 2004; Meira et al., 2015).

The knowledge of the granites outcropping near southern limit of the ET is scarce. Understanding the genesis, tectonic context and age may be reasonable to make a few remarks on the state of the ET evolution. Several models of tectonic evolution of the ET and consequent granite genesis are proposed: a) ET associated to the southern Brasilia Belt as an extension of the Socorro-Guaxupé magmatic arc over the Paranapanema cratonic margin (Trouw et al., 2013); (b) Embú and Paraíba do Sul basement rocks represent a paleocontinent and the most proximal terrane belonging to the allochthonous colliding upper plate of the Ribeira Belt where during the Cryogenean and Tonian different magmatic arcs were developed outboard of the São Francisco-Congo paleocontinent (Heilbron et al., 2013); (c) part of the reworked border of the Sao Francisco craton (Henrique-Pinto et al., 2014); (d) ET is a segment of an intracontinental orogen, and consequently not directly

* Corresponding author.
E-mail addresses: cr.passarelli@usp.br (C.R. Passarelli), sanjeet.verma@ipicyt.edu.mx (S.K. Verma).

https://doi.org/10.1016/j.lithos.2019.05.024
0024-4937/

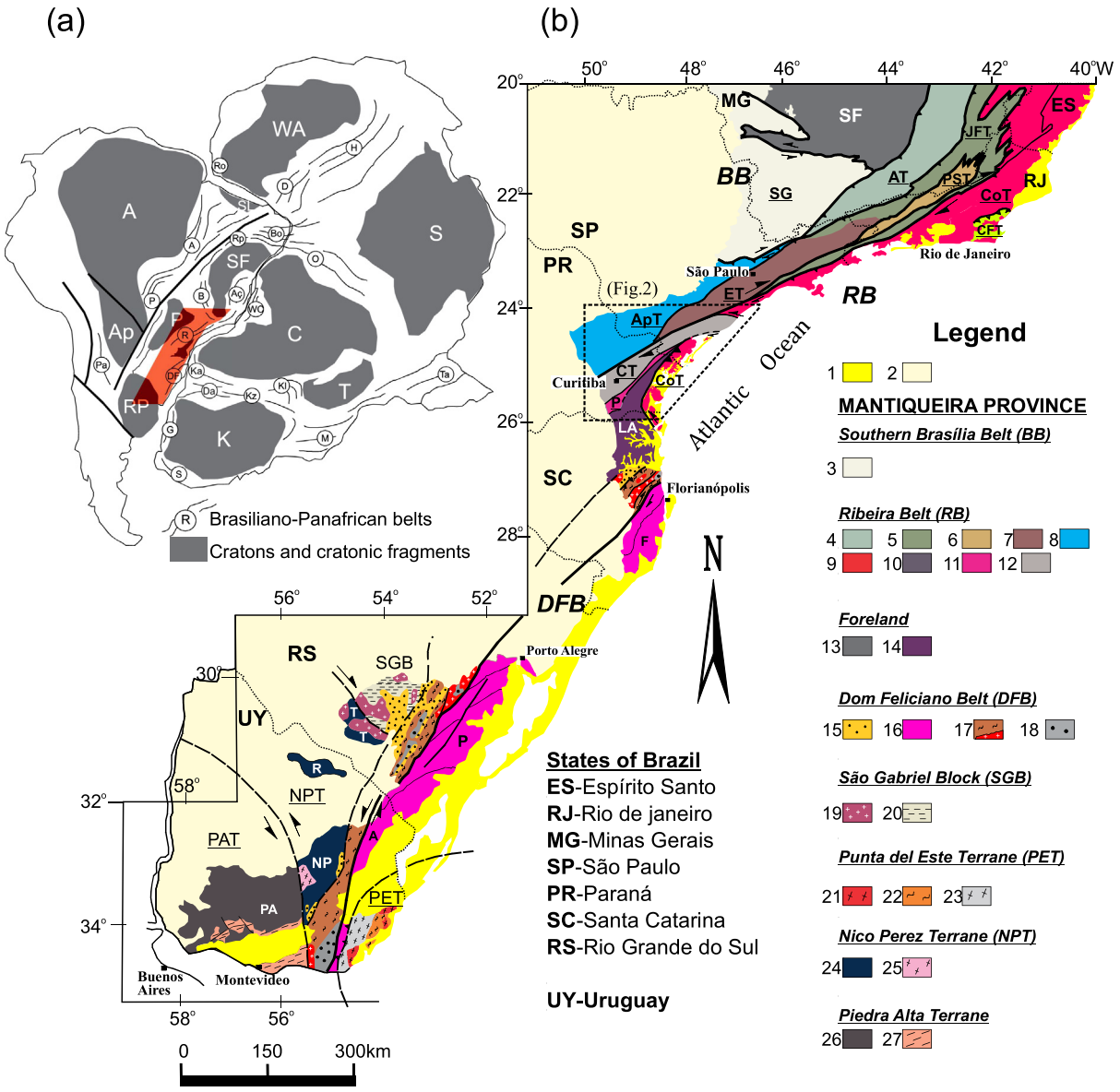

Fig. 1. (a). Reconstruction of West Gondwana after Heilbron et al., 2008; Vaughan and Pankhurst 2008; Frimmel et al. 2011 and Cordani et al. 2013, showing cratonic and Brasiliano–Panafrican components. Cratons shown in grey: A, Amazonia; C, Congo; K, Kalahari; LA, Luis Alves, P, Paranapanema, SF, São Francisco; WA, West Africa. Brasiliano–Panafrican belts (ringed): Bo, Borborema; Rp, Rio Preto; A, Araguaia; Aç, Araçuaí; P, Paraguai; B, Brasilía; R, Ribeira; DF, Dom Feliciano; Pa, Pampean; H, Hoggar; D, Dahomey; Ro, Rockelides; O, Oubangides; Ta, Tanzania; WC, West Congo; Ka, Kaoko; Da, Damara; K/Z, Katangan/Zambezi; KI, Katanga-Lufilian Arc; M, Mozambique; G, Gariep; S, Saldania. Location of the Mantiqueira Province is shown. (b) General outline of the Mantiqueira Province (Brazil-Uruguay). Simplified from Basei et al. 2000; Heilbron et al. 2004a; Passarelli et al., 2011; Tupinambá et al., 2012. Location of Fig. 2 is show. 1. Quaternary and Tertiary sediments; 2. Paraná Basin (PB). MANTIQUEIRA PROVINCE - NORTHERN DOMAIN: Brasília Belt (BB): 3. Socorro-Guaxupé nappe; Ribeira Belt (RB): 4. Andrelândia Terrane (A); 5. Juiz de Fora Terrane (JF); 6. Paraíba do Sul Terrane (PS); 7. Embu Terrane (E); 8. Apiaí Terrane (Ap); 9. Coastal Terrane (Co) –Oriental, Rio Negro / Mongaguá /Paranaguá-Iguape Domains, Iguape Metassediments. 10. Cabo Frio Terrane (CF); 11. Piên Magmatic Arc (P); 12. Curitiba Terrane (CT). Foreland units: 13. S. Francisco Craton and Cover (SF). 14. Luis Alves Terrane (LA); SOUTHERN DOMAIN - Dom Feliciano Belt (DFB): 15. Ediacaran-Cambrian Basins. 16. Granite belt: Florianópolis (F), Pelotas (P), Aiguá Batholiths (A); 17. Schist Belt and intrusive granitoids: Metamorphic Complexes and granitoids: Brusque (Santa Catarina State), Porongos (Rio Grande do Sul State) and Lavalleja (Uruguay); 18. Basement Inliers. São Gabriel Block (SGB): 19. Intrusive granitoids; 20. Metamorphic rocks. Punta del Este Terrane (PET): 21. Intrusive granites; 22. Rocha Group; 23: Cerro Olivo Complex. Nico Perez terrane (NPT): 24. Archean-Paleoproterozoic granulites and gneiss (Taquarembó - T, Rivera - R, Nico Perez – NP); 25. Illescas intrusive rapakivi granite. Piedra Alta Terrane (PAT): 26. Paleoproterozoic granitoids and gneisses (Piedra Alta - PA); 27. Supracrustal belts.

related to ocean consumption and related plate convergence in the Neoproterozoic (Meira et al., 2015); (e) Ediacaran magmatism in the ET have been formed in a continental magmatic arc setting, as an inner belt of plutons derived from reworking of Paleoproterozoic crust, but if magmatism is associated with subduction and whether or not the ET corresponds to a microplate and is unrelated to the São Francisco paleoplate is open to doubt (Alves et al., 2016).

This paper reports the results of U—Pb age dating by laser ablation and inductively coupled mass spectrometry (LA-ICP-MS) of zircon grains from the Juquiá (JG) and Sete Barras (SBG) granites, both intrusive into metasedimentary rocks near the southern limit of the ET. We also present an integrated geochemical and isotopic study of granites and petrographic information of the intruded metasedimentary sequence. The definition of the magmatic evolution and tectonic setting of the ET will be supporting a new paleogeographic reconstruction of the Gondwana during part of the Proterozoic Eon.

2. Geological setting

RB is a subduction-to-collisional belt developed consequently of the collision between the São Francisco, Paranapanema, Luís Alves and Congo Cratons and the assembly of West Gondwana during the

Neoproterozoic (e.g., Basei et al., 2010; Brito Neves et al., 1999, 2014; Campanha and Brito Neves, 2004; Trouw et al., 2013). It consists of several tectonic domains, limited either by thrust or by transpressive shear zones (Fig. 1b), which were juxtaposed in Ediacaran time. The northern and central RB comprise the Occidental, Paraíba do Sul-Embú, Oriental (Coastal Terrane or Serra do Mar Microplate) and Cabo Frio terranes (Heilbron et al., 2004; Tupinambá et al., 2012). Apiaí, Embú and Curitiba terranes compose the southern RB (Basei et al., 2009; Campos Neto,

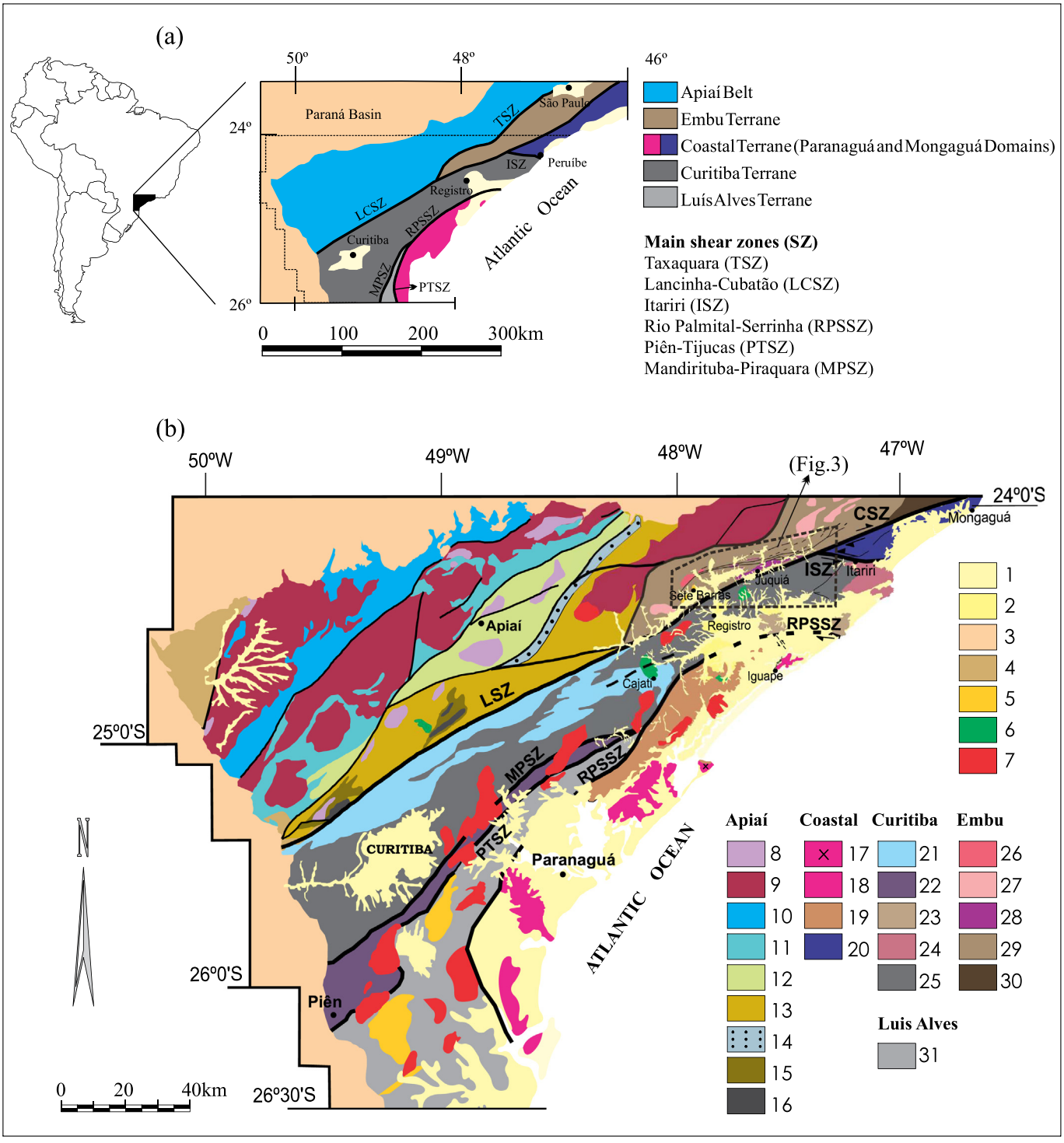

Fig. 2. (a) Tectonic sketch of the southern Ribeira Belt; (b) Simplified geological map of the southern Ribeira Belt. 1. Quaternary sediments; 2. Tertiary sediments; 3. Paraná Basin; 4. Eopaleozoic basins; 5. Neoproterozoic basins; 6. Cretaceous alkaline rocks 7. Graciosa Suite alkaline granites. Apiaí Terrane. 8. Neoproterozoic granitic stocks. 9 Neoproterozoic calc-alkaline granitic batoliths (Cunhaporanga, Três Córregos, Agudos Grandes). Açungui Supergroup: 10. Itaiacoca Group; 11. Água Clara Formation; 12. Lageado Subgroup; 13. Votuverava Formation; 14. Iporanga Formation; 15. Perau Formation; 16. Granite-gneisses nuclei. Coastal Terrane. *Paranaguá/Iguape Domain*: 17. Cardoso Island granite-sienitic suite; 18. Paranaguá Batolith; 19. Rio das Cobras and Iguape Sequences. *Mongaguá Domain*: 20. Itariri Complex and intrusive granites undifferentiated. Curitiba Terrane. 21. Capirú Formation; 22. Piên-Mandirituba Batolith; 23. Cachoeira Sequence; 24. Itatins Complex; 25. Atuba-Registro Complexes. Embu Terrane. 26. Sete Barras granite; 27 indifferentiated syn-orogenic granites; 28. Juquiá type granite; 29. Embu Terrane; 30. Rio Capivari Complex orthogneisses. Luís Alves Terrane. 31. Santa Catarina granulitic Complex. Main shear zones (SZ). RPSSR: Rio Palmital-Serrinha; PTSZ: Piên-Tijucas; MPSZ: Mandirituba-Piraquara; TXSZ: Taxaquara; LC: Lancinha-Cubatão; MASZ: Morro Agudo; RSZ: Ribeira; FSZ: Figueira; QASZ: Quarenta Oitava; ISZ: Itapirapuã.

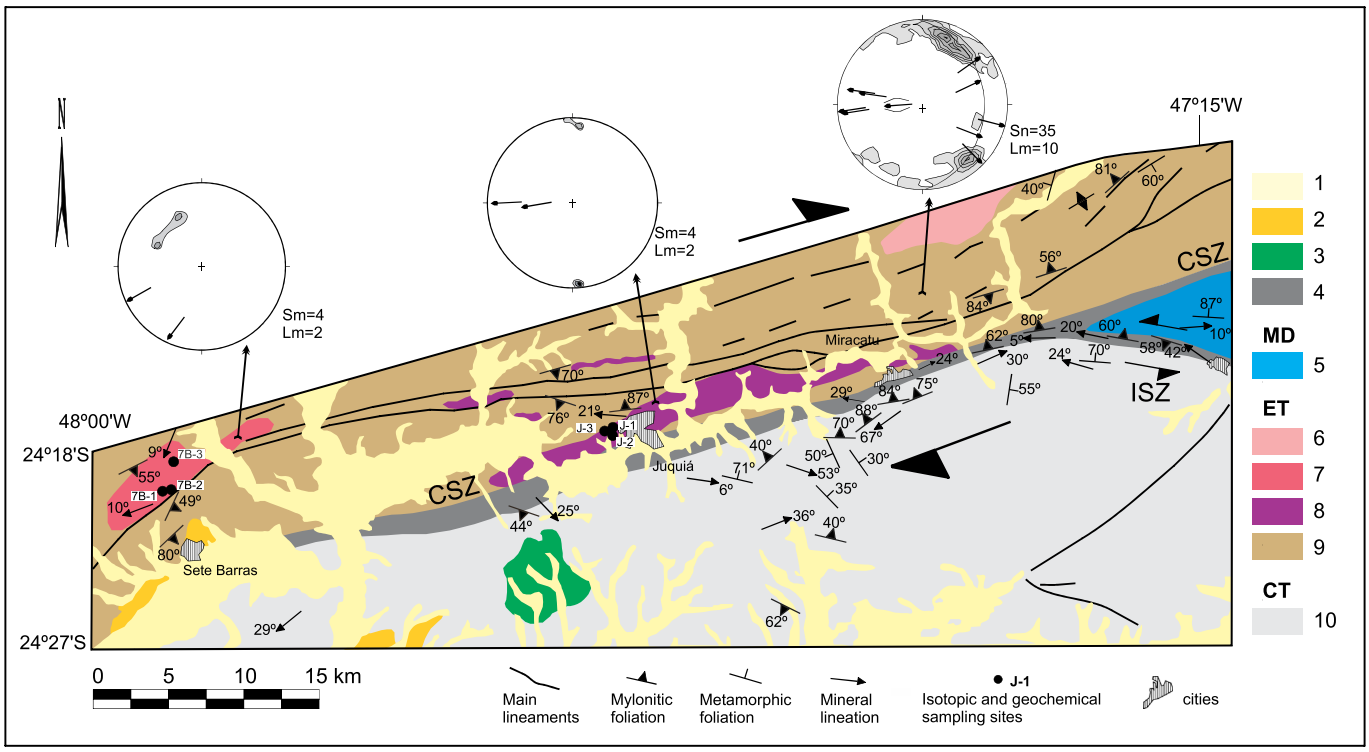

Fig. 3. Geological setting of the studied area. Stereograms of main foliation attitude (mylonitic) for granites and metasedimentary rocks. 1. Recent deposits; 2. Tertiary deposits; 3. Cretaceous Juquiá Alkaline rocks; 4. Mylonitic rocks. Mongaguá Domain (MD): 5. Gneiss-migmatitic rocks, granites. Embu Terrane (ET): 6. Indifferentiated syn-orogenic granites; 7. Sete Barras granite; 8. Juquiá granite; 9. Metasedimentary Rocks. Curitiba Terrane (CT) (Registro Complex): 10. Gneiss-migmatitic rocks. ISZ: Itariri Shear Zone, CSZ: Cubatão Shear Zone.

2000; Siga Jr. et al., 2011a, 2011b) where the Lancinha-Cubatão and Itariri shear zones (ISZ) separate the supracrustal terranes to the north (Embu and Apiaí terranes) from the granite-gneissic migmatitic terranes to the south, including the Coastal (CoT) and Curitiba (CT) terranes (Fig. 1b).

2.1. The Embu Terrane (ET)

The ET is entirely bounded by major shear zones, and is located among the following terranes (Fig. 2a–b). (1) Apiaí Terrane (AP) comprises metavolcanosedimentary sequences, including deposits from 1.8 to 1.4 Ga passive margin and Ediacaran continental sedimentary basins (Juliani et al., 2000; Basei et al., 2003, 2010; Campanha et al., 2008, 2016; Siga Jr. et al., 2009, 2011a, 2011b. (2) Curitiba Terrane (CRT) represents the internal domain of the southern RB and include Paleoproterozoic gneiss and migmatites that is intensively deformed and migmatized during the Neoproterozoic (Passarelli et al., 2018). (3) The Coastal Terrane (CoT), which includes the Oriental Domain, as defined by Heilbron et al. (2008), and the Paranaguá/Iguape (Cury et al., 2008; Passarelli et al., 2004) and Mongaguá Domains (Passarelli et al., 2016). The latter domain hosts one or more Neoproterozoic magmatic arcs. Based on geophysical constraints and geological, geochemical and geochronological compilation, Bruno et al. (2018) reinforce the similarities between the Brusque, Paranaguá and Florianópolis terranes (Fig. 1b). Different tectonic models propose the RB to represent an east-trending subduction associated to the closure of the Adamastor Ocean at 580 Ma (e.g., Basei et al., 2018; Heilbron et al., 2013). A simpler tectonic model where the RB evolved in an intracontinental environment between two subduction and collisional systems, rather than through multiple collision events between independently drifting terranes (Meira et al., 2015).

The ET in SE of São Paulo State (Fig. 3) comprises predominantly mica schists and paragneiss partially migmatized, intruded by the Juquiá and Sete Barras granitic plutons. Steep dipping dextral NE mylonitic zones crosscut the terrane.

The interpretation of the ET as a separate "exotic" terrane attached to the NE domain of the RB (Paranapiacaba Orogen) during the late Brasiliano collage (Alves et al., 2013; Brito Neves et al., 1999; Campos Neto, 2000; Cordani et al., 2002; Heilbron et al., 2004; Vlach, 2001) is primarily based on igneous and metamorphic ages of 805–790 Ma (Campanha et al., 2019; Cordani et al., 2002; Vlach, 2001), which are significantly older than most Neoproterozoic ages of the RB. Additionally, the predominance of felsic granites with peraluminous character in the ET is notable, and typical metaluminous granites are almost absent (Alves et al., 2016) in contrast to the plutons in the adjacent terranes. An alternative interpretation, based on U—Pb zircon ages on the Serra do Quebra-Cangalha Batholith suggests that the ET is the continuation of the Socorro-Guaxupé Nappe (Fig. 1b) and part of the active margin of the Paranapanema paleocontinent (Duffles et al., 2016; Trouw et al., 2013). Another scenario based on U—Pb zircon ages from metaigneous and metasedimentary rocks of the ET and CoT is proposed by Meira et al., 2015 where a common tectonic history for the two domains rather than isolated terranes is more plausible.

The ET is composed of a Paleoproterozoic basement, a metasedimentary sequence, and Neoproterozoic intrusive granitoids, today mostly orthogneisses in its southern part. The Rio Capivari Complex (RCC) is recorded in the northern portion of ET and comprises the stretched Paleoproterozoic basement inliers composed mainly of metatexitic orthogneisses of ca. 2.2 Ga reworking of Archean (~2.7 Ga) rocks, and amphibolitic rocks, consistently reworked by the Brasiliano Orogeny (Babinski et al., 2001; Maurer et al., 2015; Meira et al., 2015). Isotopic evidences suggest that the RCC was not the basement of the

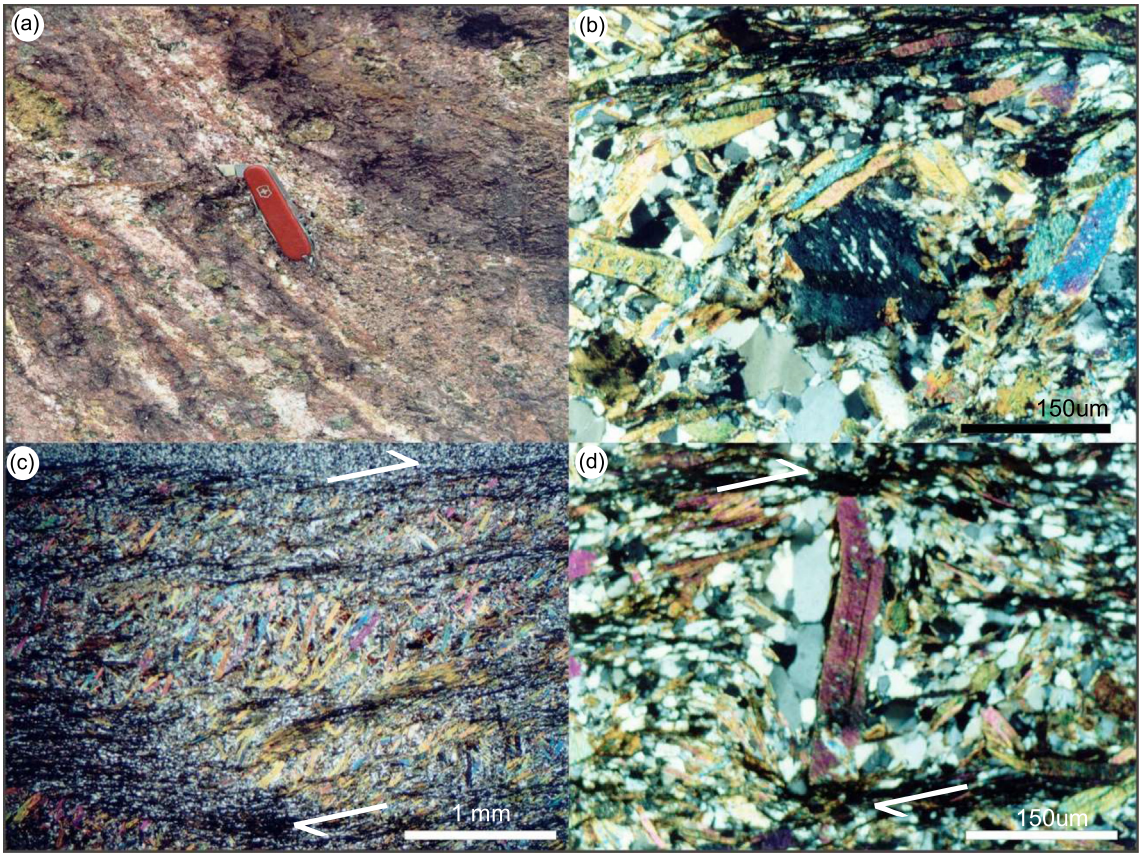

Fig. 4. (a) Field photograph of weathered garnet-biotite-schists with centimeter-scale quartz-feldspar leucosomatic bands; (b-d) photomicrographs of cordierite-biotite-muscovite quartz schist in XZ sections; (b) photomicrographs of cordierite with poikiloblastic texture with quartz inclusions; (c) asymmetrical shear bands indicating a dextral sense of movement; (d) Recrystallized quartz in pressure shadow adjacent to muscovite porphyroclast indicating a dextral sense of movement.

metasedimentary sequence of the ET (Benetti Silva, 2017). In the NW portion the metasedimentary sequence is composed mainly by partially migmatized mica schists, paragneiss and quartzite (Cordani et al., 2002); fine-grained mica schist, phyllite with subordinate quartzite, metabasite and calc-silicate rocks defined as Miracatu Sequence (Dantas et al., 1987) predominate in the southern portion. The maximum and minimum ages of sedimentation of the metasedimentary rocks defined in an easterly part of the ET is around 1.0 Ga and 660 Ma respectively (Benetti Silva, 2017; Costa et al., 2017; Duffles et al., 2016; Meira et al., 2015). In the southwestern ET, the interval of sedimentation is delimited between 970 Ma and 850 Ma (Campanha et al., 2019). Several Ediacaran granitic bodies with predominantly high-K calc-alkaline and peraluminous signatures intrude these units (Alves et al., 2016).

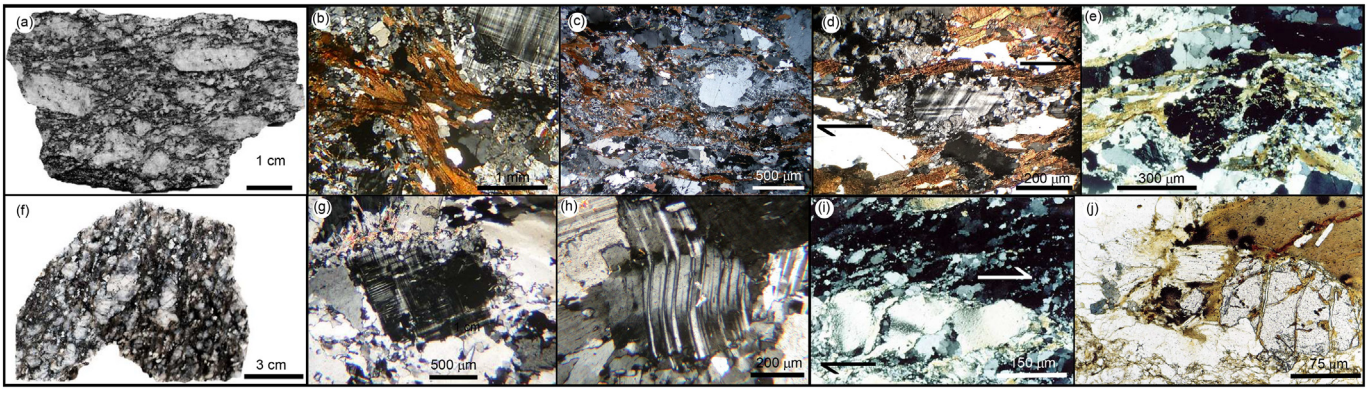

Fig. 5. Granites hand samples and photomicrographs. (a) Protomylonitic two mica Juquiá granite (JG); (b–e) photomicrographs of JG in cross-polarized light XZ sections: (b) myrmekite at the margins of the K-feldspar crystal and mylonitic foliation marked by concentrations of well-oriented biotite; (c) recrystallization of K-feldspar in the matrix together with segregate quartz and well-oriented biotite; (d) K-feldspar porphyroclast with dextral sense of shear, recrystallized 'mortar' texture and asymmetric pressure shadow filled with recrystallized quartz; (e) garnet porphyroclast with asymmetric pressure shadow filled with recrystallized quartz and biotite; (f) Protomylonitic tourmaline-garnet-two mica Sete Barras granite (SBG); (g–j) photomicrographs of SBG: (g) microcline crystal with mortar texture (cross-polarized light YZ section); (h) bent twin lamellae in plagioclase (cross-polarized light XZ section); (i) sigmoidal muscovite porphyroclast with dextral sense of shear (cross-polarized light XZ section); (j) fractured garnet filled by quartz, anhedral blue tourmaline; and damage halo in biotite around monazite crystals (plane-polarized light YZ section). (For interpretation of the references to colour in this figure legend, the reader is referred to the web version of this article.)

Table 1
Whole-rock major-trace and rare earth element data from the studied samples. Major elements in (wt%) and trace and rare earth elements in (ppm). * Duplicate analysis.

	Juquiá granite			Sete Barras Granite			
Sample	J-1	J-2	J-3	7B-1	7B-2	7B-3	7B-3*
SiO_2	70.43	71.55	71.86	75.95	75.47	73.62	73.62
TiO_2	0.33	0.322	0.284	0.03	0.029	0.091	0.091
Al_2O_3	14.25	13.61	14.16	13.49	13.5	14.1	14.1
Fe_2O_3	3.20	3.08	2.67	1.23	1.25	1.36	1.36
MnO	0.09	0.094	0.074	0.03	0.036	0.063	0.063
MgO	0.820	0.820	0.700	0.040	0.040	0.150	0.150
CaO	2.41	2.36	2.19	0.47	0.46	0.81	0.81
Na_2O	2.85	2.52	2.76	4.03	3.57	4.12	4.12
K_2O	4.53	4.34	4.43	4.68	4.88	4.82	4.82
P_2O_5	0.14	0.131	0.113	0.03	0.042	0.066	0.066
LOL	0.64	0.65	0.51	0.56	0.58	0.75	0.75
TOTAL	99.69	99.48	99.75	100.55	99.86	99.95	99.95
Mg#	34.07	35.27	34.62	4.95	4.85	16.1	16.1
Al(K + Na + 2Ca)	4.88	8.81	16.01	18.05	29.19	11.98	11.98
Fe + Mg + Ti	64.59	62.98	54.39	16.78	17.02	21.91	21.91
A/CNK	1.02	1.04	1.06	1.07	1.13	1.05	1.05
A/NK	1.49	1.54	1.52	1.15	1.21	1.18	1.18
Ba	420	389	326	23	25	142	142
Rb	211	196	184	477	502	433	434
Sr	244	235	218	9	10	49	48
Zr	296	266	239	62	53.2	87.4	76.4
Nb	23	23	26	24	26	29	31
Ni		5	8				
Co	5	36			51		
Zn	47	42	37	42	45	51	51
Cs	7	7	9	8	9	19	19
Ta	2.2			3.1			
Hf	7.8	7.83	7.16	2.5	2.95	3.37	2.99
Sc	7			4			
V	26	34	29				
Th	39.2	39.4	38.5	15.1	16.8	19.1	20.1
U	6.73	7.31	5.89	23.4	29.8	18.0	18.4
Pb	37.5	37.6	32.0	27.0	42.8	35.0	34.9
F		523	368		1656	2450	2450
Tl	1.45			2.48			
Mo							
W	0.9			1.8			
Sn	5			11			
Ga	16	15	15	23	25	25	25
Y	18	17	17	66	75	44	42
La	63.9	69.5	70.3	20.3	21.5	30.8	31.5
Ce	129	136	114	44	45	66	69
Pr	13.9	15.0	14.6	5.4	5.97	7.45	7.70
Nd	44.0	50.4	49.5	17.9	21.2	27.0	27.6
Sm	6.89	7.48	7.82	5.92	6.88	6.60	6.65
Eu	1.15	1.25	1.31	0.105	0.12	0.37	0.38
Gd	4.41	4.30	4.80	5.88	8.47	6.23	5.99
Tb	0.57	0.55	0.60	1.58	1.87	1.21	1.20
Dy	2.78	2.96	3.01	10.0	11.7	7.12	7.03
Ho	0.55	0.57	0.58	2.02	2.41	1.44	1.33
Er	1.62	1.53	1.48	5.71	6.38	3.70	3.54
Tm	0.26	0.23	0.20	0.948	1.02	0.57	0.56
Yb	1.60	1.55	1.26	5.65	6.72	3.84	3.63
Lu	0.207	0.23	0.19	0.752	0.90	0.52	0.50

Table 2
Whole-rock major-trace and rare earth element data from the geochemical reference samples from Geological Survey of Japan (GSJ): JB-1a Basalt - Kitamatsuura basalt; JG-1a Granodiorite - Sori granodiorite; JG-3 Granodiorite - Mitoya granodiorite; JR-1 Rhyolite - Wada Toge obsidian. Major elements in (wt%) and trace and rare earth elements in (ppm). M = measured values; R = recommended values; sd = standard deviation; DL = detection limits.

Sample	JB1a			JG 1a			
	M	R	sd	M	R	sd	DL
SiO_2	52.35	52.16	0.13435	72.22	72.19	0.0212	0.03
TiO_2	1.284	1.3	0.01131	0.254	0.25	0.0028	0.003
Al_2O_3	14.61	14.51	0.07071	14.18	14.22	0.0283	0.02
Fe_2O_3	9	9.1	0.07071	1.99	2.05	0.0424	0.01
MnO	0.146	0.15	0.00283	0.059	0.06	0.0007	0.002
MgO	7.71	7.75	0.02828	0.68	0.69	0.0071	0.01
CaO	9.29	9.23	0.04243	2.13	2.13	0	0.01
Na_2O	2.8	2.74	0.04243	3.25	3.41	0.1131	0.02
K_2O	1.41	1.42	0.00707	4	4.01	0.0071	0.01
P_2O_5	0.259	0.26	0.00071	0.085	0.08	0.0035	0.003
LOL	1.1	1.1	0	0.59	0.59	0	
TOTAL	99.96	99.72		99.44	99.68		
Ni	144	140	2.82843	9	6.4	1.8385	5
Co	37	39.5	1.76777	6	5.7	0.2121	6
Zn	81	82	0.70711	38	38.8	0.5657	2
Sc	30	27.9	1.48492	< 14	6.31		14
V	200	220	14.1421	27	23	2.8284	9

Sample	JG-3			JR-1			
	M	R	sd	M	R	sd	DL
Ba	469	466	44	48.2	50.3	10.2	0.5
Rb	64.0	67.3	7.3	241	257	16	0.01
Sr	373	379	29	27.4	29.1	5.2	0.01
Zr	131	144	12	90.5	99.9	6.3	0.03
Y	15.6	17.3	1.5	40.0	45.1	5.2	0.01
Nb	6.81	5.88	0.85	18.0	15.2	1.7	0.02
Cs	1.96	1.78	0.22	18.8	20.8	2.6	0.01
Hf	3.78	4.29	0.41	4.69	4.51	0.67	0.01
Th	7.92	8.28	0.65	26.4	26.7	2.6	0.01
U	2.41	2.21	0.41	8.25	8.88	1.32	0.01
Pb	11.5	11.7	1.4	18.6	19.3	3.8	0.02
La	22.1	20.6	2.2	20.0	19.7	1.77	0.01
Ce	43.5	40.3	4.8	46.5	47.2	4.3	0.01
Pr	5.14	4.70	1.24	6.08	5.58	0.69	0.01
Nd	19.0	17.2	1.8	24.1	23.3	2.8	0.01
Sm	3.30	3.39	0.44	5.75	6.03	0.81	0.01
Eu	0.84	0.90	0.08	0.28	0.3	0.041	0.01
Gd	2.99	2.92	0.28	5.49	5.06	1.05	0.01
Tb	0.43	0.46	0.05	0.92	1.01	0.2	0.01
Dy	2.55	2.59	0.53	5.87	5.69	1.06	0.01
Ho	0.55	0.38	0.16	1.33	1.11	0.24	0.01
Er	1.56	1.52	0.36	3.89	3.61	0.91	0.01
Tm	0.24	0.24	0.05	0.66	0.67	0.071	0.01
Yb	1.69	1.77	0.35	4.46	4.55	0.46	0.01
Lu	0.26	0.26	0.05	0.68	0.71	0.08	0.01

3. Mineralogy and Petrography

The extremely weathered metasedimentary rocks include garnet-mica-quartz schists, occasionally migmatized (Fig. 4a), subordinate quartzite, and local boudins of calc-silicate rocks. Local occurrences of cordierite mica-schists indicate medium-high temperature and low- to medium-pressure metamorphism.

The compositional layering (S_0) and parallel foliation (S_1) were almost completely transposed into a S_2 foliation, normally parallel to a mylonitic foliation (Sm). Both foliations are slightly folded by a later phase (S_3) foliation with fold axis B_3 plunging 50-60° to S80-88 W parallel to mineral stretching lineations (stereogram, Fig. 3). Mylonitic foliation is parallel to the main metamorphic foliation S_2. In thin section of the schists folia or thin parallel layers of muscovite, biotite interleaved with recrystallized quartz define a well-defined foliation (S_2). Garnet or cordierite (Fig. 4b) and muscovite occur as main porphyroblasts. Mylonitic schists develop asymmetrical extensional shear bands (Fig. 4c), fine-grained recrystallized quartz and sericite in pressure shadows at muscovite borders indicate dextral motion (Fig. 4d). The muscovite + biotite + quartz + cordierite assemblage indicates amphibolite facies.

The Sete Barras (SBG) and Juquiá (JG) monzogranites are intrusive into the metasedimentary rocks and are elongated according to the shear zones (trend of the major axis around N70E), especially the JG. The protomylonitic textures, more pronounced in the JG (Fig. 5a), are characterized by the sigmoidal K-feldspar porphyroclasts and orientation of mafic minerals. The NE to E-W mylonitic foliation (Sm) with sub-vertical to moderate dip towards SE contain a biotite and feldspar stretching lineation with gentle plunges to SW and W (stereograms, Fig. 3). In the SBG the geometric relation between the foliation orientation (NE dipping to SE), the plunging of the stretching lineation to SW

and the dextral kinematic indicators are compatible with a predominance of local transtensional movement.

The Juquiá pluton is formed by protomylonitic, porphyritic granite (Fig. 5a), which contains quartz + two feldspars + biotite + muscovite. Garnet, zircon and monazite (almost completely replaced by epidote) occur as accessory minerals. In thin sections, the protomylonitic foliation is expressed mainly by comminuted K-feldspar and plagioclase, segregated bands of quartz and aligned biotite and muscovite (Fig. 5b–c). Asymmetric pressure shadows, mica fish, shear bands, and σ-type porphyroclasts of K-feldspar yield a dextral sense of shear. Quartz grains have undulatory extinction, and tend to segregate into ribbons and to very fine-grained dynamically recrystallized zones (Fig. 5c). Porphyroclasts of microcline with recrystallized 'mortar' texture (Fig. 5b) are common, although well-marked recrystallization occurs in the matrix together with segregate quartz (Fig. 5c). Smaller porphyroclasts of oligoclase and crystals in the matrix may have bent twin lamellae. The biotite and less abundant muscovite crystals are oriented parallel and contribute to define the Sm (Fig. 5b–c). Subeuhedral biotite with light yellow to reddish brown pleochroism is rarely altered to chlorite. Primary muscovite is characterized by large crystal sizes (ca. 300 μm) and euhedral to subeuhedral shape, and the secondary muscovites show a finer anhedral crystal size. Garnet crystals also develop porphyroclasts with asymmetric pressure shadows of recrystallized quartz and biotite (Fig. 5d).

The Sete Barras pluton consists of a protomylonitic granite (Fig. 5e) with quartz + two feldspars + biotite + muscovite. Garnet, zircon, monazite and tourmaline occur as accessory minerals. In thin section, the restrained protomylonitic foliation is defined by weak orientation of comminuted feldspar porphyroclasts and by continuous bands of quartz. These rocks contain K-feldspar and plagioclase porphyroblasts in a matrix of quartz, K-feldspar, plagioclase, biotite and muscovite. In XZ sections kinematic indicators such as mica fish, shear bands, sigmoidal mica porphyroclasts, σ-type porphyroclasts of K-feldspar yield a dextral sense of shear on moderate dipping foliation planes. The quartz grains tend to segregate into continuous bands, normally as elongate crystals with undulatory extinction and serrate grain boundaries. The dynamically recrystallized quartz suggests that basal <a> glide system (blue colour with gypsum plate) and a little prism <a> slip system (red colour with gypsum plate) were activated. Discrete recrystallized mortar texture is observed in film-type, spot and mesoperthitic microcline (Fig. 5f). Oligoclase plastic deformation is evident from bent twin lamellae and undulatory extinction (Fig. 5g). Biotite with light yellow to reddish brown pleochroism is normally subeuhedral but also interstitial. Subeuhedral to euhedral muscovite crystals also form porphyroclasts, usually with strong undulatory extinction. Garnet crystals are normally fractured and rare bluish tourmaline crystals are typically anhedral (Fig. 5h).

4. Analytical methods

The locations of the collected samples from the Juquiá and Sete Barras protomylonitic granites for geochemistry, isotope geochemistry and geochronological studies are shown in Table 1. The data were obtained at the facilities of the Núcleo de Apoio à Pesquisa (NAP) - Geoanalytic Laboratories - Geoscience Institute and the Geochronological Research Centre (CPGeo), University of São Paulo, Brazil (IGc-USP).

4.1. Whole-rock geochemical analyses

Major oxides concentrations were determined by X-ray fluorescence spectrometer (XRF) on fusion beads, and 7 g pressed powder pellets to determine selected trace elements. Geochemical Reference Materials 169 and 114 have been used for calibration of major and selected trace elements according Mori et al. (1999).

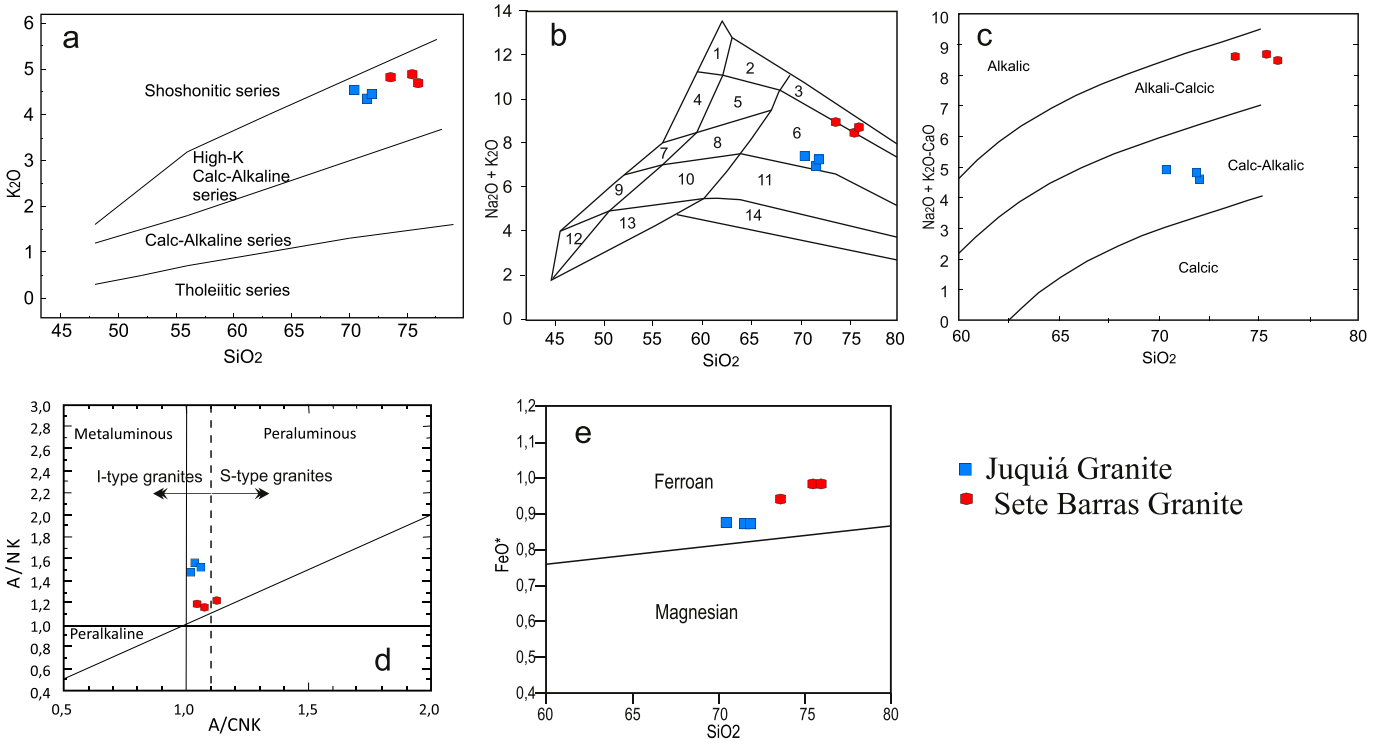

Fig. 6. (a) SiO_2 x K_2O after Peccerillo and Taylor (1976); (b) TAS classification diagram of the granitoids using the classification of Middlemost (1985): 1-alkali feldspar syenite, 2-quartz alkali feldspar syenite, 3-alkali feldspar granite, 4-syenite, 5-quartz syenite, 6-granite, 7-monzonite, 8-quartz monzonite, 9-monzodiorite, 10-quartz monzodiorite, 11-granodiorite, 12-diorite and gabbro, 13-quartz diorite, 14-tonalite; (c) Plot of $Na_2O + K_2O$–CaO (MALI) against SiO_2 showing the approximate ranges for the alkalic, alkali–calcic, calc-alkalic, and calcic rock series. Frost et al. (2001); (d) A/CNK x A/NK diagram after Maniar and Piccoli (1989), based on the Shand's index; (e) FeO* vs. SiO_2 plot. $FeO^* = FeO_{Total}/(FeO_{Total} + MgO)$. Fields of ferroan and magnesian from Frost and Frost (2008).

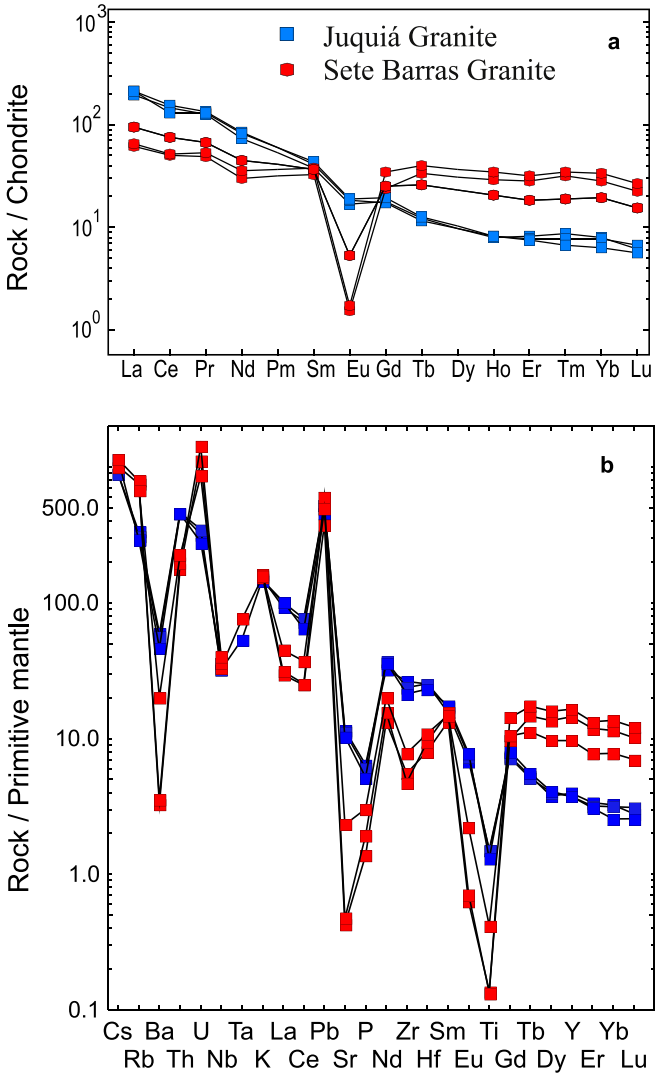

Fig. 7. (a) Chondrite normalized (Sun and McDonough 1989) REE distribution patterns; (b) Primitive mantle-normalized multi-element plot (McDonough and Sun, 1995) of Juquiá and Sete Barras granite samples.

Trace element and REE data of whole rocks were determined by ICP mass spectrometry (ICP-MS) at Institute of Geosciences, University of São Paulo, Brazil, following the analytical procedure described by Navarro et al. (2008).

The results of XRF and ICP-MS analysis is presented in Table 1. A duplicate of one sample of Sete Barras granite was made. To check the precision and accuracy of the analytical data, geochemical reference samples from Geological Survey of Japan (GSJ) were analyzed. In Table 2 is presented the measured and recommended values, with standard deviation and detection limits of both XRF and ICP-MS procedures.

4.2. Whole-rock isotopic analyses

A Finnigan MAT 262 multi-collector thermal ionization mass spectrometer was used to obtain Sr—Nd and Rb—Sr whole-rock isotope analyses. Neodymium crustal residence ages (T_{DM}) were calculated following the depleted mantle model of DePaolo (1981), and a two-stage Nd isotope evolution model was used for the calculation of the T_{DM} of DePaolo et al. (1991). εNd(t) values were calculated by using U—Pb zircon ages.

4.3. U—Pb and Hf analyses

Zircon crystals were examined using both conventional optical microscopy and cathodoluminescence (CL) microscopy. All CL images were obtained from a split screen on a FEI Quanta 250 Scanning Electron Microscope (SEM) with an Oxford Instruments XMAX CL detector in the High-Resolution Geochronology Laboratory of the GeoLab-IGc-USP. The internal structure of monazite grains was observed using an Electron Probe Microanalyzer (EPMA), equipment JEOL JXA-8530F, in the back-scattered electron images (BSE) mode at Laboratory of EPMA - NAP - Geoanalytic Laboratories. The grains were mounted in 2.5 cm diameter epoxy discs polished sufficiently to expose the internal structures of the grains.

Operating procedures were followed by Sato et al. (2011) for in situ analysis of U—Pb in zircon and monazite by LA-ICP-MS. The instruments have an Excimer 193 nm Laser (Photon Machines) coupled to a Thermo Scientific™ NEPTUNE™ MC-ICP-MS with a double-focusing multi-collector array, installed at the CPGeo–IGc-USP laboratory. The laser has a spot size of approximately 32 μm and each spot analysis took time of 45 s. All analyses were checked against zircon (GJ-1) or monazite (44069) standards. At each 50 min of analyses, four blanks, four synthetic NIST-12 standard and five GJ1 standard are measured, which are used for all corrections, one of the Mud Tank standard is performed as an unknown sample, and twelve measurements of unknown sample that complete one spread sheet. The analytical data obtained in the MC-ICP-MS are reduced and corrected with in-house software developed by Siqueira et al. (2014), using a "R" statistical package based on Python programming language. All final ages and plots were processed using the IsoplotEx software (Ludwig, 2012).

Similarly, Sato et al. (2009) have described analytical procedures for in situ Hf isotopic in zircon. The ca. 39 μm diameter laser spot required ca. 60 s of ablation time, a repetition rate of 7 Hz and He used as the carrier gas. The Lu—Hf isotopic analyses were performed on the same zircon domains that were previously U—Pb dated by LA-ICP-MS. Mass bias corrections of Lu—Hf isotopic ratios were done using the variations of GJ1 reference zircon (Table S5).

5. Results

5.1. Major elements

The Juquiá (JG) and Sete Barras (SBG) granites are characterized by high contents of SiO_2 = 70.4–75.9 wt%, Al_2O_3 = 13.5–14.2 wt%, CaO = 0.47–2.4 wt%, and P_2O_5 = 0.03–0.14 wt% (Table 1). They contain

Table 3
Sm—Nd analytical data for the Juquiá and Sete Barras granites.

ET	Sample	Sm (ppm)	Nd (ppm)	$^{147}Sm/^{144}Nd$	$^{143}Nd/^{144}Nd$	ε(0)	fSm/Nd	T_{DM} (Ma)	$\varepsilon(T_{DM})$	T1 (Ma)	ε(T1)
Juquiá	J-1	7.852	50.816	0.0934	0.511479	−22.61	−0.52	1983.8	3.52	799	−12,08
Juquiá	J-2	7.821	49.548	0.0955	0.511501	−22.19	−0.51	1989.9	3.51	799	−11,87
Juquiá	J-3	7.475	50.410	0.0897	0.511487	−22.45	−0.54	1913.1	3.67	799	−11,54
S. Barras	7B-1	6.882	20.829	0.1998	0.511950	−13.42	0.02	2260.1	−13.66	602	−13,66
S. Barras	7B-2	6.876	21.190	0.1962	0.511952	−13.38	0.00	2240.5	−13.35	602	−13,34
S. Barras	7B-3	6.596	27.042	0.1475	0.511777	−16.79	−0.25	2220.1	−13.03	602	−13,01
S. Barras	7B-3*	6.951	27.576	0.1524	0.511777	−16.79	−0.23	2243.8	−13.40	602	−13,39

* Duplicate analysis.

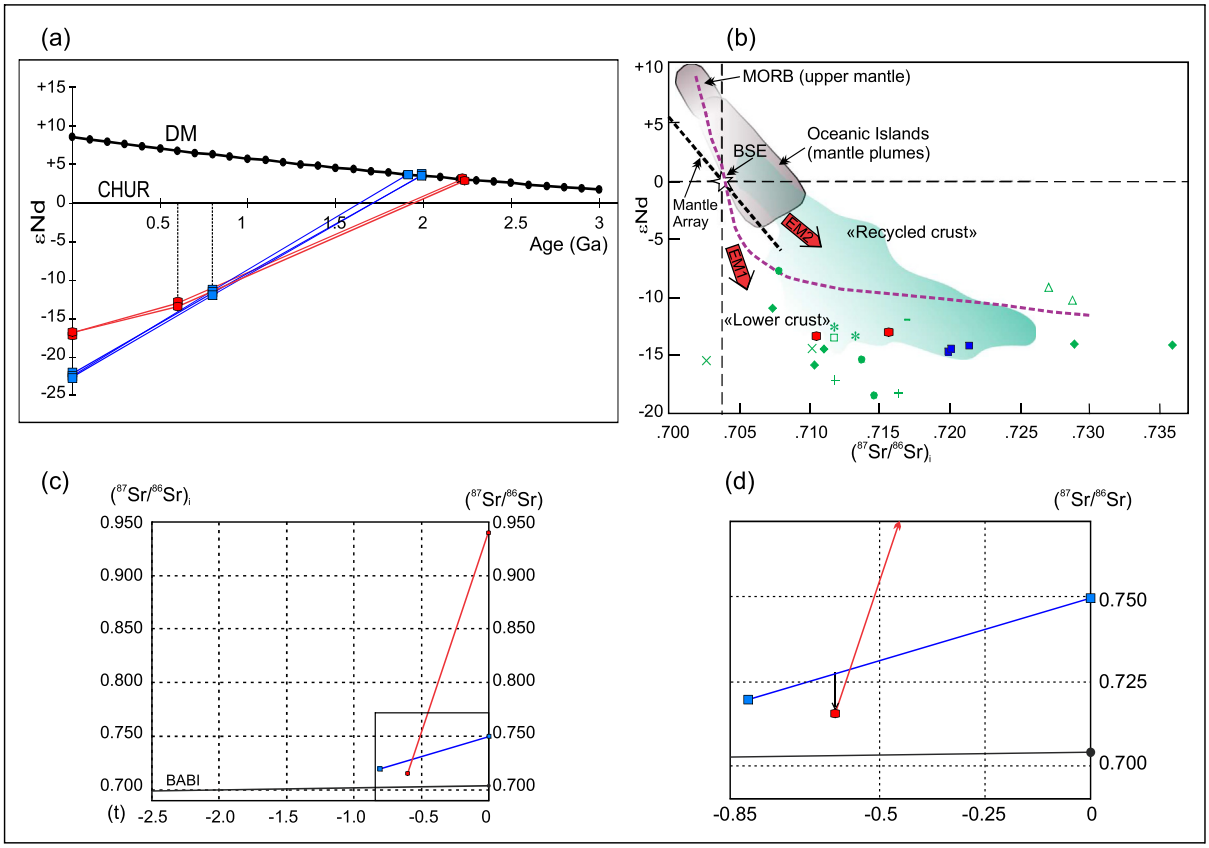

Fig. 8. Nd and Sr isotopes diagrams of JG and SBG: (a) Nd evolution diagram vs. time. Vertical dashed lines represent ages of ~800 Ma and ~600 Ma. Small red and blue solid circles correspond to εNd (t = crystallization age) of analyzed rocks. CHUR—chondritic uniform reservoir line; DM—depleted mantle line; (b) εNd_i - $(^{87}Sr/^{86}Sr)_i$ diagram for the granites with initial ratios calculated for 600 Ma (modified after White, 2015). Sr and Nd isotope ratios in marine sediments from the world oceans (Pacific, Atlantic and Indian) from Ben Othman et al., 1989, MORB— mid-ocean ridge basalts and BSE–bulk silicate Earth are shown. The mantle sources of MORB and the mantle end-members EMI (enriched mantle type I) and EMII (enriched mantle type II) are from Zindler and Hart (1986). Green symbols are of studied granites of the central ET (data from Table 2 of Alves et al., 2016 were recalculated to t = 600 Ma): Δ = S.Q. Cangalha; – = Lagoinha; • = Santa Branca; □ = Sabaúna; + = Guacuri; * = Itapeti; **x** = Mogi das Cruzes; ♦ = Mauá; (c) Evolution of $^{87}Sr/^{86}Sr$ ratio of JG and SBG; (d) detail of the square area. (For interpretation of the references to colour in this figure legend, the reader is referred to the web version of this article.)

high alkali (K_2O = 4.34–4.88 wt%; Na_2O = 2.52–4.12 wt%) and low MgO (0.04–0.82 wt%) and $Fe_2O_3^T$(1.23–3.20 wt%) contents (Table 1).

In the K_2O versus SiO_2 diagram of Peccerillo and Taylor (1976) the studied granites have a high-K calc-alkaline character (Fig. 6a) and classified in the TAS diagram (Middlemost, 1985, Fig. 6b) as granite (JG) and border-line alkali-feldspar granite (SBG). In the Modified Alkali-Lime Index (MALI, Fig. 6c) they plot in the fields of calc-alkalic (JG) and alkali-calcic (SBG). The samples are slightly peraluminous, with aluminous index ranging from 1.0 to 1.1 (Fig. 6d). For two-mica granites this result is unexpected, though typical strongly aluminous minerals are present only as accessories. These granites are typically ferroan (Frost et al., 2001, Fig. 6e) and the Fe number increases with SiO_2 content. Additionally, the Mg number (Mg#) clearly differentiates the two granites: JG has the highest Mg # between 34 and 35, while SBG shows major variations with the smallest values between 5 and 16.

5.2. Trace elements

The chondrite normalized rare earth element (REE) patterns for the three JG samples are closely grouped. They have a relatively strong LREE/HREE fractionation [La_N/Yb_N = (200/7) = 29], and negative Eu anomalies with Eu/Eu* values around 0.59 (Fig. 7a), directly comparable to those found in average upper continental crust (e.g. ~0.65 - Taylor and McLennan, 1985). The SBG samples display lower LREE/HREE fractionation, (La_N/Yb_N = 60/13) = ~5 and remarkable HREE enrichment, with values of Tb ~26 and Yb ~13 (Fig. 7a), with strong negative Eu anomaly (Eu/Eu* = 0.05). This indicates the tendency to gradual decrease of LREE and relative increase of HREE in most evolved silica-rich facies, typical of highly evolved granites. Primitive mantle-normalized multi-element patterns (McDonough and Sun, 1995, Fig. 7b) display negative Nb anomalies with a positive Pb anomalies (Fig. 7b); these features are attributed to the difference in the property

Table 4
Rb–Sr analytical data for the Juquiá and Sete Barras granites. Samples 7B1 and 7B-2 have very low Sr contents.

ET	Sample	Rb (ppm)	Sr (ppm)	$^{87}Rb/^{86}Sr$	$^{87}Sr/^{86}Sr$	ε (0)	T_{DM} (Ma)	e(T_{DM})	T1(Ma)	ε(T1)	$(^{87}Sr/^{86}Sr)_i$
Juquiá	J-1	211.0	244.0	2.513	0.74865	626.7	1312.6	−22.68	809	228.23	0,71,998
Juquiá	J-2	183.7	217.8	2.450	0.74813	619.4	1331.8	−22.55	809	231.22	0,72,018
Juquiá	J-3	196.4	235.3	2.426	0.74908	632.8	1373.0	−22.28	809	248.75	0,72,141
S. Barras	7B-3	433.0	49.1	26.100	0.93975	3339.2	639.0	−27.09	595	205.79	0,71,567
S. Barras	7B-3*	434.4	48.2	26.698	0.93975	3339.2	624.7	−27.18	595	133.67	0,71,054

* Duplicate analysis.

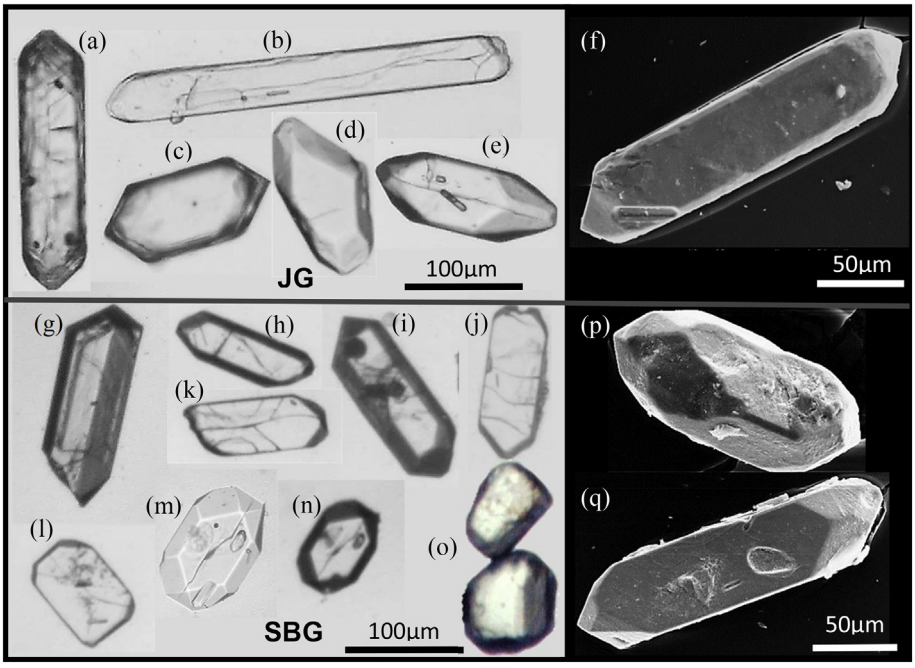

Fig. 9. External morphology variations of zircon and monazite crystals from studied granites. JG: (a) to (e) transmitted light images of zircon crystals. (f) Secondary electron image showing typical zircon morphology. SBG: (g) to (n) transmitted light images of zircon and (o) monazite crystals. (p) and (q) SEI showing two typical zircon morphologies from the SBG. (SEI) with EHT = 20 KV, obtained with the LEO 440I SEM - Scanning Electron Microscopy Laboratory of the IGc-USP.

of metasomatic agents (hydrous melts and supercritical fluids) derived from subducting crustal rocks.

5.3. Sm—Nd and Rb—Sr isotopic data

Whole rock Sm—Nd analyses (Table 3, Fig. 8a) indicate minor differences in εNd_t between the two granites, while the model ages are rather different. The SBG shows lower εNd_t (−13 and − 13.4) and some slightly older T_{DM} model ages (2.2 Ga) compared to the JG with εNd_t values between −11.5 and – -12 and 1.9 Ga T_{DM} model age. For the SBG samples the f_{SmNd} factor deviates of the −0.45 ± 0.10 interval and additional chemical fractionation of Sm—Nd would have taken place, therefore a two-stage Nd isotope evolution model was used for the calculation of the T_{DM} (DePaolo et al., 1991). Nd model ages of the granites and their strongly negative initial εNd values indicate that the magmas were derived from Paleoproterozoic rocks with a relatively long crustal residence time.

In the Sr—Nd isotope diagram (Fig. 8b); along with the data for oceanic island basalts and MORB sample major reservoirs in the mantle, both granites fall in the continental crust field enriched quadrant. In the same diagram, additional data are plotted for the comparative study. These granites data were taken from Alves et al. (2016) from central part of the ET.

The very low Sr concentrations of samples 7B-1 and 7B-2 of SBG did not allow the determination of $^{87}Sr/^{86}Sr$ isotope ratio, and the same sample (JB-3), in particular, shows a relatively wide variation in $(^{87}Sr/^{86}Sr)_i = 0.71567–0.71054$ (Table 4). The JG exhibits higher initial $^{87}Sr/^{86}Sr$ ratio, extended from 0.719981 to 0.72141 (Table 4), and both granites show flat correlation with Nd isotopes. Despite uncertainties related to the high Rb/Sr ratios of the SBG samples, the isotopic

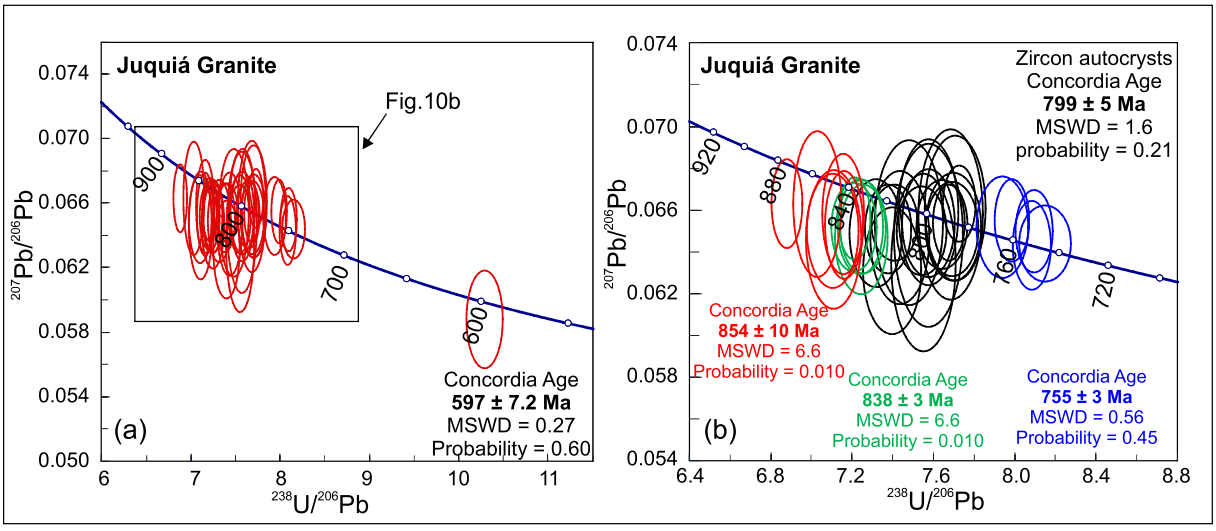

Fig. 10. (a) concordia diagram for U—Pb isotope ratios of zircons from the JG measured by LA-ICP-MS. Error ellipses of individual spots are 2σ; (b) Detailed Concordia plot of the mostly concordant zircons.

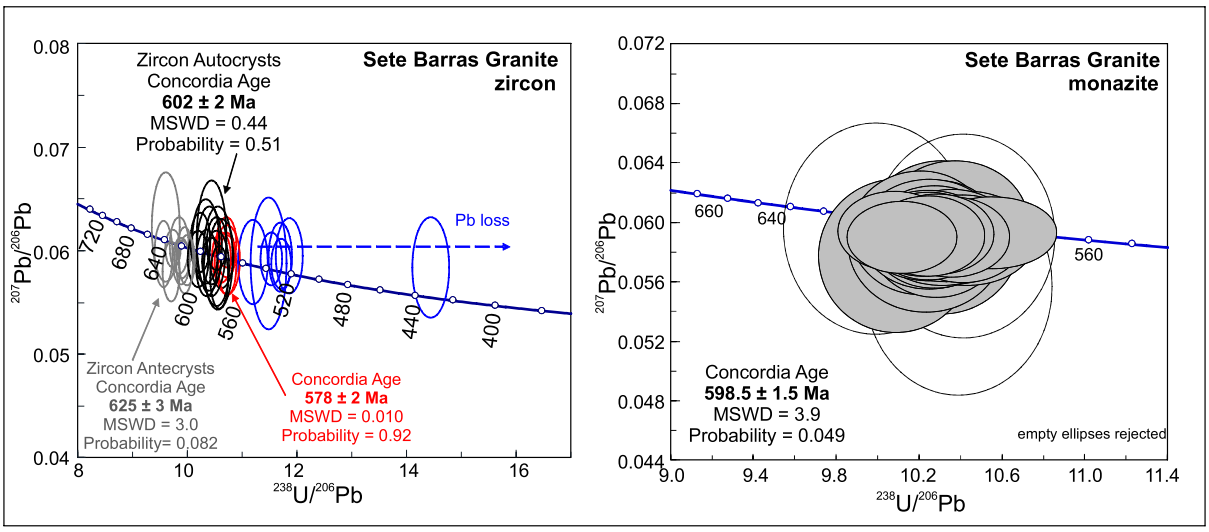

Fig. 11. (a) concordia diagram for U—Pb isotope ratios of zircons; (b) monazites from the SBG measured by LA-ICP-MS. Error ellipses of individual spots are 2σ.

compositions of the SBG are quite similar to those Ediacaran granites of the central ET (Sabaúna, Itapeti, Mogi das Cruzes and Mauá), while the JG are strongly differed.

The $^{87}Sr/^{86}Sr$ evolution diagram (Fig. 8c–d) indicates not only different sources but also distinct evolution for the granites, where the SBG was probably contaminated by much evolved sources during its evolution. The high value of initial $^{87}Sr/^{86}Sr$ ratio for the JG (0.71961) corroborates the enriched character of this granite source (Table 4).

5.4. Zircon U—Pb (LA-ICP-MS) geochronology

5.4.1. External morphology and surface features

Zircon crystals from JG samples are normally transparent, subeuhedral to euhedral prismatic grains with aspect ratio 3:1 to 5:1, while the pyramidal faces are normally under-developed (Fig. 9a–f). Growth zones, mineral inclusions of different sizes and some fractures (Fig. 9a–e) are observed. Some typical P4 and P5 Pupin subtypes (Pupin, 1980) are common (Fig. 9a–b) and more rarely the subtypes S20 (Fig. 9c) and S13, S14 (Fig. 9d–e), the latter characterized by steep pyramids. The typical zircon morphology of the JG is represented in conventional images and secondary electron images (SEI) (Fig. 9f), marked by well-developed surfaces with only some small scratches and roughening. The pyramidal tops are not mechanically damaged.

Zircon crystals of SBG are quite short, prismatic grains (2:1 to 3:1) which are transparent, light brownish, subeuhedral, and are rarely unfractured or inclusion-free (Fig. 9g–q). Some typical P1 (Fig. 9g–h) or G1 Pupin subtypes (Fig. 9i–l) are common, and S18 (Fig. 9m–n) of higher temperature zircon (Pupin, 1980) are rare. Monazite grains recovered from SBG are subeuhedral to euhedral, transparent, and bright yellow (Fig. 9o). The SEI images for two typical zircon morphologies of the SBG show (Fig. 9p) S4 Pupin subtype grains where roughening and scratches are more prominent and (Fig. 9q) almost pristine P1 Pupin subtype grains.

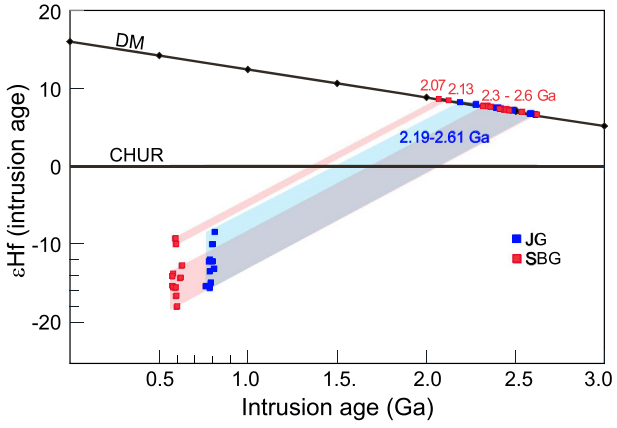

Fig. 12. εHf(t) versus intrusion age diagram for zircon grains from the Juquiá (JG) and Sete Barras (SBG) granites. The blue and red bands indicate the range of the Hf TDM model ages for the JG and SBG respectively. The evolution trends were calculated for a $^{176}Lu/^{177}Hf$ of 0.0113. DM-depleted mantle evolution line, CHUR-chondritic uniform reservoir. (For interpretation of the references to colour in this figure legend, the reader is referred to the web version of this article.)

5.4.2. Internal structures and ages

The most common pattern observed in the analyzed crystals is the oscillatory zoning that represents the heterogeneous distribution of trace elements (Hoskin, 2000). Figs. S1–S2 (see supplementary materials) show selected zircon cathodoluminescence (CL) images from both granites.

Both blurred primary zones and preserved growth zones are common, although homogeneously textured zircon crystals occur in JG (Fig. S1). Presence of transgressive zones of recrystallization (e.g. crystals 4, 11, 15, 20; Fig. S1), local development of convolute primary zoning (e.g. crystals 3, 8, 13; Fig. S1), and complex growth zoning with possible local intermediate resorption in zircon also occur (Fig. S1, spot 1.1).

The analyzed zircon crystals of SBG (Fig. S2a) preserved oscillatory zoning due to magmatic growth, blurred primary zones, locally with possibly inherited cores, and transgressive recrystallization zones (Corfu et al., 2003). Development of local convolute zoning is rare, and homogeneous zircon crystals are very uncommon. In BSE images, most monazite grains display an unzoned internal structure (Fig. S2b). Some monazite crystals show a patchy zonation (crystals 14 and 18; Fig. S2b) and magmatic zonation preserved (crystals 20 and 23; Fig. S2b).

The results of the new LA-ICP-MS U—Pb analyses are presented in Tables S1–S4, including the summary of U—Pb reference GJ-1 zircon data obtained during the period when analyses were done (see supplementary materials) and Figs. 10a–b and 11a–b. All data is presented as Concordia age with 1σ, decay-constants errors included, MSWD (of concordance) and probability (of concordance).

The results for analyzed zircon crystals from the JG are summarized in Table S1. Concordant zircon age dispersion is observed in the JG (Fig. 10a). The larger set of data provide a Concordia age of

799 ± 5 Ma (Fig. 10b) interpreted as crystallization age which, despite a small difference, agrees with previous ID-TIMS age of 793 ± 3 Ma (Passarelli et al., 2011). Two different sets of zircons with older ages of 853 Ma (crystals 6, 21, 27, 30 and 34; Fig. S1) and 833 Ma (crystals 12, 17, 23, 25 and 29; Fig. S1) are separated from the main set. The CL images of the zircon crystals that provide 853 Ma ages show a complex and non-unique texture. They include zircon grains with homogeneous domains (crystals 6 and 21; Fig. S1), transgressive recrystallization fronts (zircon 6, non-dated); zircons with core and rim, both with older ages (zircon 27; Fig. S1) and zircons with possibly inherited euhedral cores with convolute zones (non-dated, zircon 30; Fig. S1) or homogeneous unzoned (spot 34.2; Fig. S1) with

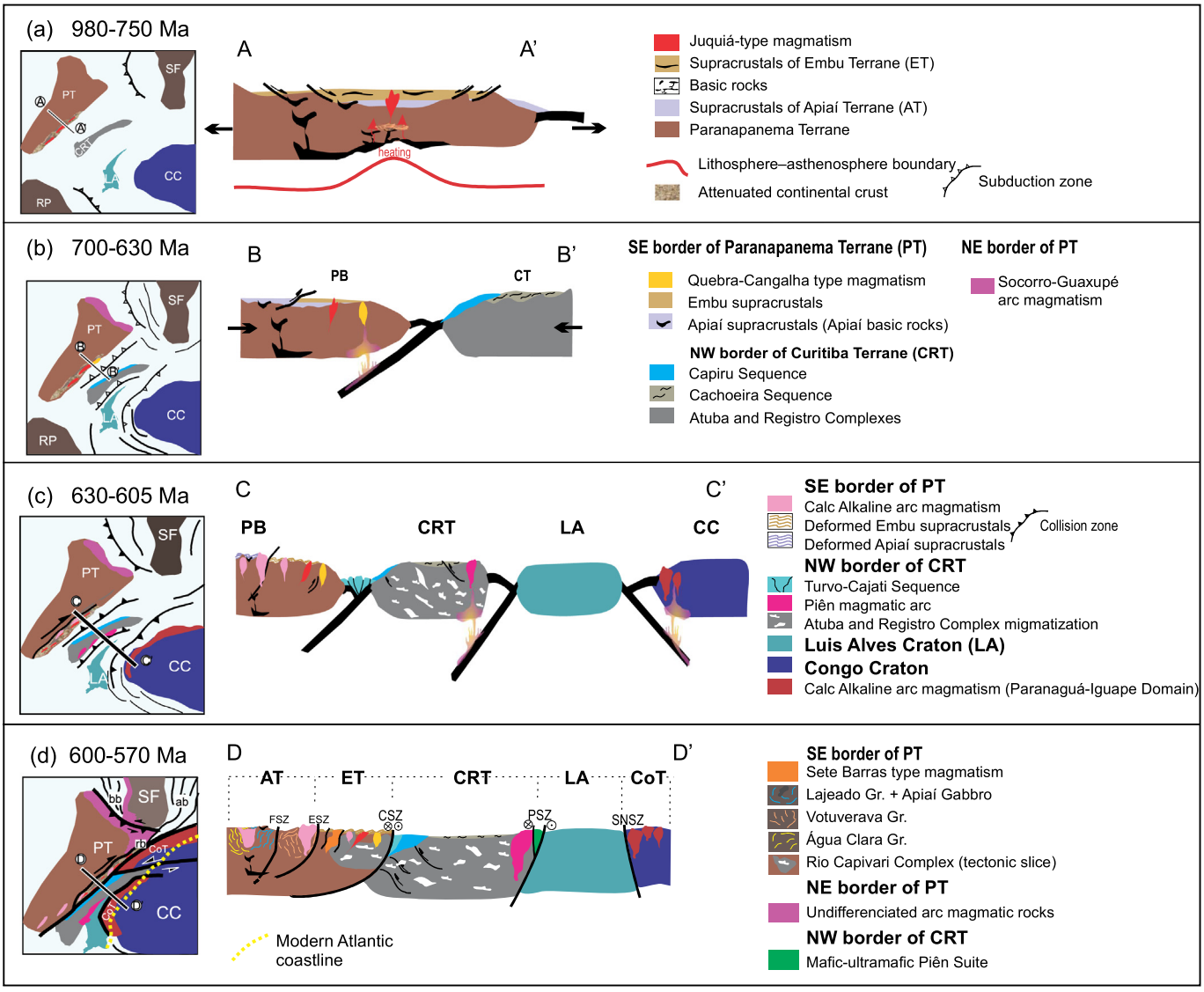

Fig. 13. Paleogeographic reconstruction of the West Gondwana assembly and schematic NW–SE sections from the southern Ribeira Belt. Simplified tectonic model showing the main geological units that were juxtaposed during collisions associated with the Gondwana formation. (a). 980–750 Ma. Main tectonic regime: divergence/transtension. SE border of Paranapanema Terrane. Basement rocks of the Embu Terrane (ET) and Apiaí Terrane (AT): (i) Tigre, Betara and Apiaí basement nuclei: Paleoproterozoic ages with 1,75 Ga syenogranites (1); (ii) Mesoproterozoic supracrustals rocks of Apiaí Terrane - Água Clara Formation (1550-1500 Ma), Votuverava Group (1480 Ma), Lajeado Group (1200-880 Ma) and lower Itaiacoca Group (> 1000 Ma) (2); (iii) Embu Terrane: supracrustal rocks with young detrital zircons of ca. 850 Ma (3) and main amphibolite metamorphism at 790 ± 20 Ma (4); (iv) Juquiá-type magmatism: 800 Ma peraluminous granite (this work). (b). Main tectonic regime: convergence/transpression. SE border of Paranapanema Terrane: (i) Calc-alkaline and S type magmatism - Quebra-Cangalha and Santa Catarina Granite: 680-660 Ma to 630 Ma (5, 6); (ii) Thrusting to N and/or SW with maximum age of 660 Ma (7); (iii) Metamorphism at 750 Ma and 705 Ma in Tonian granites and supracrustal rocks of ET (8); (iv) Apiaí Terrane continental supracrustals - Abapã Sequence - Itaiacoca Group deposition: 645-628 Ma (9). NE border of Paranapanema Terrane: Socorro-Guaxupé arc (680-630 Ma) (10). NW border of Curitiba Terrane (CT) and Rio Capivari Complex: (i) Infrastructure of CRT: Archean-Paleoproterozoic rocks. Atuba Complex (PR state) - orthogneisses, migmatites and amphibolitic rocks of 2.2 Ga and 2.0 Ga; Registro Complex (SP State)- orthogneisses, migmatites and amphibolitic rocks of 2.2-2.1 Ga and 1.4 Ga (11, 12); Rio Capivari Complex: (SP State) orthogneisses and amphibolitic rocks of 2.4 Ga; 2.2 Ga and 2.0 Ga (13); (ii) Amphibolite to granulite facies metamorphism at Cachoeira Sequence – CRT (14); (iii) Capiru and Turvo Cajati sequences - sedimentation ages between 0.8 and 0.6 Ga, probably maximum depositional age 650 Ma (15). (c): Main tectonic regime: convergence / transpression. SE border of Paranapanema craton: (i) Calc-alkaline magmatism: Santa Catarina Granite (630 Ma); Agudos Grandes (610 Ma), Três Córregos, Cunhaporanga Batholits (620–590 Ma) (6); (ii) AT continental supracrustals: Abapã Sequence: (645–630 Ma) (16); (iii) Accrescionary prism (Turvo-Cajati Sequence): 650-630 Ma (17). NW border of Curitiba Terrane: (i) Piên magmatic arc – 620-610 Ma (18); (ii) Atuba Complex (2.2–2.0Ga) (19); (iii) Cachoeira Sequence: minimum age of sedimentation: 750 Ma (12); (iv) Metamorphism and partial melting at Rio Capivari Complex (20) and Atuba and Registro Complexes at 620–590 Ma (19, 12). Luis Alves Craton: (i) 2.7 Ga (TTG igneous activity); 2.3–2.1 Ga (high-grade metamorphism); 1.8 Ga (regional cooling) (21). Coastal terrane (Paranaguá and Mongaguá Domains): 2.1 Ga Paleoproterozoic polycyclic basement; Neoproterozoic supracrustals; Ediacaran arc magmatic rocks (22). (d): Main tectonic regime: convergence / transpression. (i) Closure of the Adamastor Ocean (23): orogenic collage between PT, CRT and Luis Alves craton; (ii) Mafic-ultramafic Piên Suite (632 Ma): remnants of obducted oceanic floor (24); (iii) Sete Barras type magmatism: 600 Ma (this work): final stages of the closure of the ocean; (iv) 590-580 Ma peak of peraluminous granite magma generation in northern Embu Terrane (not represented in figure) (25). FSZ: Figueira shear zone; ESZ: Embu shear zone; CSZ: Cubatão suture zone; PSZ: Piên suture zone; SNSZ: Serra Negra suture zone. References in Fig. 13: (1–25; see supplementary material SR1).

oscillatory zoned rim with older age (zircon 30; Fig. S1) or much younger age (spot 34.2; Fig. S1). The same complex textures are observed in zircons that provide 833 Ma: a) crystals with homogeneous unzoned core (crystals 12, 23; Fig. S1) and younger rims (784 and 727 Ma) with apparent oscillatory zonation; b) crystals with homogeneous unzoned mantle (zircon 17; Fig. S1) with transgressive recrystallization front (non-dated); c) recrystallization front (zircon 25; Fig. S1) in possibly older inherited core; and d) oscillatory zoning rim in a oscillatory zoning inherited core (zircon 29; Fig. S1). Another cluster of age around 755 Ma refers to both resorption, metamorphic rim and oscillatory zoned zircon domains (crystals 2, 4, 14, 28, 33; Fig. S1). A concordant age around 600 Ma was obtained in homogeneous unzoned high CL intensity spot on zircon with complex growth zoning, with local metamorphic resorption in core and in planar growth banding overgrowth (spot 1.1; Fig. S1).

New results for zircon crystals from the SBG are presented in Table S2. Besides the distribution of the analyses all over the concordia ranges from 578 Ma to 625 Ma $^{206}Pb/^{238}U$ ages, important sets of data could be defined through statistical treatment plus CL image analysis. The larger set of data provide a concordia age of 602 ± 2 Ma interpreted as crystallization age (Fig. 11a). Some crystals with older ages (625 Ma) are meaningfully separated from the main set and are interpreted as antecrysts (Miller et al., 2007) (crystals 11, 12, 13, 22, 31; Fig. S2). Another cluster of age around 578 Ma corresponds to zircon crystals with metamorphic growth and resorption zoning (crystals 1, 4, 5, 9, 17, 18, 24, 27 and 30; Fig. S2). The CL images of the studied crystals exhibit clearly inherited nuclei (crystals 8, 11, 12, 15, 16, 20, 23, 29 and 35; Fig. S2).

New LA-ICP-MS U—Pb monazite analyses reported in Table S4 and indicates a crystallization age of 598 ± 2 Ma (Fig. 11b). The unimodal distribution of monazite analyses is similar to the zircon age, and may reflect the crystallization period of the granite, since there is no evidence of its metamorphic origin or metamorphic overgrowth.

5.5. Lu—Hf analysis of zircon

Lu—Hf analyses were carried out by LA-ICP-MS at points as close as possible of U—Pb spot analyses (Figs. S1 and S2) in the same CL sector of the zircon crystal allowing the calculation of εHf and Hf T_{DM} values at the time of crystallization. Zircon Hf T_{DM} model ages are usually referred to as crust formation ages (Hawkesworth and Kemp, 2006). The Lu—Hf isotope compositions for 22 grains from analyzed samples and reference GJ-1 zircon are summarized in Table S5, organized by granite types. Typically, for zircon, average $^{176}Lu/^{177}Hf$ ratios are very low, ranging from 0.00038 to 0.001119 for the JG and from 0.000689 to 0.004220 for the SBG.

Zircon crystals from the JG show mean values of the $^{176}Hf/^{177}Hf_{(t)}$ isotopic composition ranging from 0.282025 to 0.281840, that corresponds to a total variation of about seven ε-units [$\varepsilon Hf_{(t)} = -8.4$ to -15.6]. An average of Hf T_{DM} model ages of 2.48 Ga, and $\varepsilon Hf_{(t)}$ values around −13.4 were acquired on JG zircons. Slightly less negative values found in sections with heterogeneous zoning (e.g. spot 8.1 Fig. S1) were not considered in calculating the average. Zircon crystals from the SBG show a similar variation in $^{176}Hf/^{177}Hf_{(t)}$ isotopic composition, from 0.282142 to 0.281890, that corresponds to a total variation of about eight ε-units [$\varepsilon Hf_{(t)} = -9.2$ to -17.9]. An average of Hf T_{DM} model

Table 5
Summary of the tectonic evolution of the Embu Terrane.

Event/Interpretation	Unit-Characteristics	Method	Age (Ma)
Regional cooling/cessation of regional metamorphism-deformation	Orthogneiss – EC	WR-feldspar Rb-Sr	560
Metamorphism	Medium grade schists – EC	U-Pb zr LA-ICP-MS	570
Metamorphism/collisional phase RB	Schist - ES - metamorphic rims -	U-Pb zr LA-ICP-MS	576–574
Metamorphism/collisional phase RB[a]	SB - zircon metamorphic growth –	U-Pb zr LA-ICP-MS	578
Metamorphism/ transpressive collision	JG	U-Pb-TIMS epidote	598
Metamorphism/collision RCC + ET	RCC, orthogneiss; paragneiss – EC	U-Pb zr LA-ICP-MS	595–575
Metamorphism[a]	JG – local metamorphic resorption	U-Pb zr LA-ICP-MS	600
Magmatism[a]	A2-Type alkali-calcic peraluminous granite - SB	U-Pb zr mz LA-ICP-MS	602–598
Metamorphism/granitogenesis	Migmatitic orthogneiss-metamorphic rims - RCC	U-Pb zr LA-ICP-MS	620–590
Magmatism /magmatic arc	calc-alkaline magmatism	U-Pb zr LA-ICP-MS	615–600
Metamorphism/collision ET + PSF	RCC, orthogneiss; paragneiss EC	U-Pb zr LA-ICP-MS	615–605
Metamorphism/continental collision PC + SFC: Brasilia belt	Metamorphic rims in the schist sample – ES	U-Pb zr LA-ICP-MS	621–599
Magmatism/ ET + PSF convergence	RCC, orthogneiss; paragneiss – EC	U-Pb zr LA-ICP-MS	630–610
Early magmatic pulse[a]	Zircon antecrysts – SB	U-Pb zr LA-ICP-MS	625
Magmatism/magmatic arc, post-collisional or crust-derived granite	Metaluminous granite	U-Pb zr LA-ICP-MS	630
Early magmatic event[a]	Inherited nuclei xenocryst – SB	U-Pb zr LA-ICP-MS	640
Magmatism/magmatic arc, post-collisional or crust-derived granite	Peraluminous granite	U-Pb TIMS mz .	660
Metamorphism/continental magmatic arc	Schist and quartzite -metamorphic overgrowth – ES	U-Pb zr LA-ICP-MS	670–640
Metamorphism	Orthogneiss – EC	U-Pb zr LA-ICP-MS	705–660
Metamorphism[a]	metamorphic rim growth – JG	U-Pb zr LA-ICP-MS	755
Magmatism/Extensional Event	Meta-aplite veins and strongly foliated metagranite – EC	U-Pb zr SHRIMP	780–770
Magmatism/magmatic arc	Orthogneiss – EC	U-Pb zr LA-ICP-MS	781–788
Amphibolite metamorphism/convergent tectonic processes	Gneiss-EC; schist – ES	U-Pb zr LA-ICP-MS; EPMA mz	805–790 Ma
Magmatism/Extensional Event[a]	A1-Type calc-alkalic peraluminous granite – JG	U-Pb zr LA-ICP-MS	800
Metamorphism	Medium grade schists – EC	U-Pb zr LA-ICP-MS	810–570
Magmatism/magmatic arc	Orthogneiss – EC	U-Pb SHRIMP	811
Early magmatic pulse/Extensional Event[a]	Zircon antecrysts – JG	U-Pb zr LA-ICP-MS	850–830
Sedimentation	High grade schists – EC	U-Pb zr LA-ICP-MS	850–810
Magmatism/intraoceanic arc to collision	Migmatitic ortogneiss protoliths - RCC	U-Pb zr LA-ICP-MS	2400; 2200; 2100; 2000
Mantle/crust differentiation[a]	JG, SBG	Lu-Hf zr LA-ICP-MS	2500–2400

EPMA–Electron probe micro-analyzer; zr–zircon; mz–monazite; LA-ICP-MS–Laser Ablation Inductively Coupled Mass Spectrometry (LA-ICP-MS). RB—Ribeira Belt; BB—Brasília Belt; RCC—Rio Capivari Complex; EC—Embu Complex; ES—Embu Sequence; PC—Paranapanema Craton; SFC—São Francisco Craton; PSF—Paranapanema-São Francisco Protocontinent; JG—Juquiá granite; SBG—Sete Barras granite.

[a] Data from this work.

ages of 2.38 Ga, and $\varepsilon Hf_{(t)}$ values around −14.2 were found. Values obtained in spots that may indicate mixed areas of recrystallized rims with magmatic zonation (spot 6.1, Fig. S2) and diffuse zoning (spot 14.1, Fig. S2) were not considered in the average calculations. The negative $\varepsilon Hf_{(t)}$ values imply derivation from a source with much lower Lu/Hf ratio than the chondritic reservoir, i.e., the sources of zircon crystals for both granites have clearly crustal affinities. The range in $\varepsilon Hf_{(t)}$ values in both granites (see Table S5, Fig. 12) may suggest a similar crustal source for both and/or little modification of crustal melts. The igneous protoliths for both granites have almost similar Hf model ages (2500 Ma for JG and 2400 Ma for SBG), which indicates that mantle rocks were added to the continental crust in Siderian times. The negative values of Epsilon (Hf) are perfectly justified.

6. Discussion and interpretation

6.1. Implications from whole rock geochemical and isotopic data

The Juquiá type is best described as a ferroan calc-alkalic peraluminous two-mica granite, while the Sete Barras type is a ferroan alkali-calcic peraluminous two-mica granite (Fig. 6). The strongly negative εNd_t and εHf_t values, high initial $^{87}Sr/^{86}Sr$ ratios and the upper crust as the main source combined with its Paleoproterozoic T_{DM} ages indicate that both magmatism is characterized by crustal evolved signatures with sources of long crustal residence. Nevertheless, the geochemical and isotopic data indicate different sources and distinct evolution for the granites, where the SBG was probably contaminated by much evolved sources during its evolution.

The Juquiá-type magmatism is related to provision and melting of crustal materials deep enough to leave garnet-rich residues and the Sete Barras-type magmatism whose melting was probably shallower, involving garnet-bearing sources, generating a more evolved magmatic composition and garnet-poor residues.

6.2. Implications from U—Pb geochronological data

The crystallization age of the JG is 799 ± 5 Ma while the older ages (853 and 833 Ma) could come from antecrysts crystallized from earlier magmatic pulses. Ages of ca. 755 Ma and 597 Ma recorded in some zircon resorption domains could result from recrystallization due to the thermal overprint. Upper tonian ages are already associated with main metamorphic event in metasediments of the ET.

U—Pb zircon yielded age of the SBG is 602 ± 2 Ma and monazite 598 ± 2 Ma. Some zircons with older ages (625 Ma) may represent crystallization from an earlier pulse of magma recycling during successive magmatic injections. Younger ages zircon rims (578 Ma) correspond to a later episode where metamorphic growth and resorption occurs in the presence of a fluid phase.

6.3. Tectonic implications

This study together with the available geochronology data from Neoproterozoic rocks related to rifting event, arc magmatism and metamorphic events (Mantiqueira Province – Brazil and Uruguay; Brasília Belt and southwestern African belts-Table S6) supported some implications for the tectonic evolution of the ET and adjacent terranes.

The investigations involve the fragmentation of Rodinia and the amalgamation of West Gondwana and the opening and closing of a number of oceans, which are thought to have existed, especially northern and southern Adamastor or Brazilide Ocean (between Nico Perez Terrane/Rio de La Plata Craton and Kalahari and Congo cratons), Goiás Ocean (between São Francisco-Congo and Amazon cratons and Paranapanema block) and Charrua Ocean (between the Rio de La Plata Craton and the Nico Perez Terrane).

6.3.1. Tonian period and tectonic setting of ET (items of Table S6 is referred)

The depositional age of the supracrustals of the ET is constrained to several intervals based on youngest detrital grains and metamorphic zircon overgrowths. Data from the eastern part of the ET indicate depositional age of 980–800 Ma and 850–786 Ma (item nº. 1), whereas in the southern part an interval of depositional age 970–850 Ma is obtained (item nº. 2). Tonian ages of magmatic and metamorphic events also have been reported in the ET (items nº 3 to 10) and the geodynamic context of these old events, which is not recorded in adjacent terranes, is not well understood. Despite the scarce petrographic and geochemical data, considering the juxtaposition of the innumerous allochthonous terranes in the area, these events were interpreted to be related to an early convergent episode of arc magmatism in the evolution of the closure of the Adamastor Ocean (Alves et al., 2013; Cordani et al., 2002). On the other hand, 780–760 Ma foliated metagranite in ET (item nº. 3) is conjectured in an extensional tectonic environment and lithospheric thinning rather than through subduction and collisional processes. Although still sparse and lacking a broad meaning and characterization, it is possible to consider that between ca. 850 and 780 Ma a sedimentary basin was active and between 800 and 750 Ma important magmatic and metamorphic events must have occurred.

Older tonian ages (items nº. 15 and 16) are also recorded in the Apiaí Terrane as minimum depositional age of the Itaiacoca and Lageado Sequences with associated basic rocks, and initial break-up of continent masses with formation of the Brasiliano oceans. Additionally, in the central Ribeira Belt, a minimum depositional age of ca. 840 Ma is recorded in the Oriental Domain (item nº. 18) and remnants of a low-to-medium-K 790 Ma tonalitic banded gneiss can be recognized among the 630 Ma Rio Negro magmatic arc (item nº. 19).

A high amphibolite facies metamorphic tonian event (750–740 Ma) is also recorded in the paragneiss of the Cachoeira Sequence (Curitiba Terrane) considered being supracrustal remains of volcanosedimentary sequences (item nº. 21).

In the Andrelândia Megasequence, Brasília Belt (item nº. 23) Tonian ages are related to rifting events that culminate in the break-up of Rodinia Supercontinent with individualization of the São Francisco paleo-continent in a passive margin environment. On the other hand, between ca. 900 to 780 Ma subduction, magmatism and terrane accretion occur because of the consumption of the Goiás oceanic lithosphere in western part of the Northern Brasília Belt (item nº. 24).

In the Dom Feliciano Belt, the occurrence of A-type mylonitic granitoids of ca. 845 Ma (item nº. 30) as tectonic slices in the Schist Belt (Brusque Group, Fig. 1b) allows inferring that this period was the rift phase of the basin that generated these metasediments. Anorogenic magmatism between 850 and 750 Ma is also evidenced in the Dom Feliciano belt in Uruguay (item nº. 31). On the other hand, older orogenies were proposed in the Dom Feliciano Belt known as the Passinho (0.89–0.86 Ga) and São Gabriel (0.77–0.68 Ga) involved in the closure of the Charrua Ocean generating an intra-oceanic arc and, subsequently, an active continental margin arc (items nº. 29, 32). The opening of this ocean is thought to started in the southwestern portion of Gondwana at 950–900 Ma (item nº. 29).

In the African counterpart (Kaoko, Damara, Gariep and Lufilian-Zambezi Belts) the rupture of Rodinia marked by rifting magmatism and volcanism (items nº. 34 to 38) characterizes the period of 840–770 Ma.

A diachronic fragmentation would have occurred in the Rodinia Supercontinent, nevertheless, according to dating of Mantiqueira Province igneous and meta-igneous rocks formed during rifting episodes, the Rodinia fragmentation commenced around 880 Ma and the ocean closure, which lead to the formation of the western part of Gondwana, probably started after 750 Ma. A pervasive period of extension and continental rifting occurred at Tonian time related to break-up of Rodinia at 850–825 to 750 Ma (Johansson, 2014; Li et al., 2008). In South America, only scarce and controversial evidences

of rifting of the Rodinia supercontinent are recorded by the separation of continental terranes diachronically between 845 and 810 and 750 Ma (Basei et al., 2010; Fuck et al., 2008; Li et al., 2008). In the Ribeira and the Araçuaí belts, evidence of formation of oceanic crust is recorded at ca. 840 Ma and ca. 815 Ma respectively (Heilbron and Machado, 2003; Pedrosa–Soares et al., 1998; Pedrosa–Soares et al., 2001). Additionally, some data of rift-related siliciclastic and bimodal volcanic rocks preserved in the schist belts from Rio de la Plata/Paranapanema and Congo/Kalahari cratonic margins suggest a continental rifting phase between 900 and 780 Ma (Basei et al., 2009; Basei et al., 2018; Pedrosa–Soares et al., 2001).

6.3.2. Ediacaran period and tectonic setting (items of Table S6 is referred)

Some older events in the Brasiliano-Pan African cycle of granite magmatism in the ET are represented by the 680–660 Ma Serra do Quebra Cangalha batholith and the 630 Ma Santa Catarina Granite (item nº. 12). Both granites are interpreted as a product of a continental margin arc environment, of a prolonged period of oceanic plate subduction started at ca. 810 Ma. Ages between 670 and 630 Ma (items nº. 25 and 26) are also recorded in calc-alkaline orthogneisses and granites in Socorro-Guaxupé Nappe, Brasília Belt (Fig. 1b) interpreted as a magmatic arc prior to the collisional assembly of West Gondwana. Moreover, in the African counterpart calc-alkaline I type granitoids were emplaced during the period 655–630 Ma associated with a high T metamorphic event (item nº. 38).

A pervasive late Cryogenian-Ediacaran formation of magmatic arcs in active continental margins (see discussion in Basei et al., 2018) marked the end of ocean opening (items nº. 12 to 14 – ET; item nº. 17-AT; items nº. 19 and 20 – CoT; item nº. 22- CRT; items nº. 24 to 28 - BB; item nº. 33-DFB).

Between ca. 615 Ma and 580 Ma, high-K calk-alkaline and undifferentiated granites were emplaced at a number of sites of ET (items nº. 13 and 14). The tectonic situations identified include syn-orogenic and late to post-collision. A concordant epidote U—Pb age of the JG at age of 598 ± 9 Ma, interpreted as a late greenschist facies thermal event associated with CSZ movement (item nº. 8) similar to the U—Pb ages of ca. 600 Ma for the SBG (this work), is also interpreted here as a thermal overprint due to a collision between the different tectonic blocks. In addition, in this period, metamorphic overprinting is recorded in migmatitic orthogneiss of the Rio Capivari Complex (item nº. 11).

Shear zones that individualize the ET from the adjacent terranes and even those internal shear zones, develop an anastomosed pattern and may control the shape and intrusion of several granitic bodies of c.a. 590 Ma. Among all the muscovite-biotite granites of the ET, the Santa Branca granite is, until now, the only pluton that yielded a similar age to the SBG (ca. 599 Ma, Alves et al., 2013, 2016); however, the SBG is geochemically distinct from all these granites.

In the adjacent Apiaí Belt and Socorro-Guaxupé Nappe, the magmatism between 605 and 590 Ma is more consistent with a late orogenic or late-deformation tectonic setting (item nº. 28).

After these late events in the ET, orogenies continued in areas to the north. The Rio Doce "Orogeny"/ Rio Doce magmatic arc (Campos Neto, 2000; Gonçalves et al. 2014; Tedeschi et al. 2016) activity culminated around 500 Ma with the last events of the Búzios Orogeny (Schmitt et al., 2008). Post orogenic granites of this age probably generated during post-tectonic up-lift are found in Espírito Santo State (Medeiros et al., 2003). If the orogenies affected the area of our study the products would be found in the continental shelf and in foundered continental blocks adjacent to the South Atlantic coast.

6.3.3. Evolution of the Embu Terrane (ET) and correlated Belts – paleogeographic implications

The implications of the ages and tectonic environments of the studied granites of the ET for the amalgamation of West Gondwana is shown in Fig. 13. This model describes the stepwise paleogeographical reconstruction of NW–SE section from the southern Ribeira Belt covering the Paranapanema (PT), Apiaí (AT), Embu (ET), Coastal (CoT) and Curitiba terranes (CT) and the Luis Alves (LA) and Congo (CC) cratons.

- At 980–790 Ma, an extensional phase occurred involving subsidence in the PT, tholeiitic magmatism at 870–840 Ma in the AT, rifting, crustal attenuation and Embu basin sedimentation interbedded with basic rocks with emplacement of Juquiá type magmatism. Mesoproterozoic Apiaí supracrustals may be covered by the Embu basin in the middle Tonian (Fig. 13a). The PT (now hiding under Paraná Basin) and the Mesoproterozoic Apiaí Terrane rocks were possibly the source area of the Embu basin sedimentation (850–810 Ma) based on detrital zircons populations. Crustal melting of a Paleoproterozoic protolith with participation of metasedimentary rocks produced Juquiá-type magmatism at ca. 800 Ma. Metamorphism at 790 to 750 Ma affected Tonian granites and the metasedimentary sequence of the ET.
- The subduction zone was active between the PT and CRT, with Quebra-Cangalha and Santa Catarina Granite type magmatism being generated at ca. 680–660 Ma to 630 Ma in the ET (Fig. 13b). At this time, AT and the ET were possibly juxtaposed by thrust faults. Capiru sedimentation covers the Cachoeira Sequence in the CRT. Orthogneisses and amphibolitic rocks of the Rio Capivari Complex and CRT may constitute a single microplate at this time.
- Syn-orogenic calc-alkaline magmatism in the Ribeira Belt (ET and AT) took place during the juxtaposition of CRT and PT at ca. 630–605 Ma (Fig. 13c). During the closure of the Adamastor Ocean, also occurred the collision between the CRT and LA with calc-alkaline granites of Piên magmatic arc generation and the juxtaposition of the CC with all adjacent terranes, with Coastal Terrane magmatic arc generation (Rio Negro /Mongaguá /Paranaguá-Iguape Domains).
- The SBG may be associated with the collision setting related to the closure of this ocean (Fig. 13d) preceding the extensional tectonics responsible for emplacing the alkaline -peralkaline granitoids of the Serra do Mar Suite (Basei et al., 2009); and Itu Province of the Apiaí Terrane (Janasi et al., 2009) with ages in the range 590-580 Ma. The juxtaposition of CRT and LA terranes evolved with the subduction of Neoproterozoic oceanic crusts towards NW (Piên ophiolitic sequence). No ocean remnants between CRT and Ribeira Belt are recorded. The RCC may be added to the ET at this time.
- Cubatão Suture Zone (CSZ) separates the ET/AT (northwest) from the Curitiba granitic-gneissic Terrane (southeast) and the Serrinha, Serra Negra e Palmital suture zones separate the CoT from LA, CRT and ET (see Figs. 1b and 2). The sinistral Itariri Shear Zone dislocates part of the CC and the magmatic arc granites previously developed, creating the wedge configuration of the CoT to the north of the CRT (Figs. 1b and 2). The oblique component of the arrangements of the colliding tectonic blocks defined the transpressional character of this suture zone. The initial collision phase evolved to dextral transpressional shear zones (Passarelli et al., 2011). In addition, Table 5 summarizes the proposed tectonic evolution for the Embu Terrane.

7. Conclusions

- The Embu Terrane (ET) is part of the attenuated SE border of the Paranapanema block.
- The basement rocks of the ET (Rio Capivari Complex) are interpreted as part of the Curitiba Terrane, juxtaposed to the ET during the final stages of the Gondwana amalgamation.
- In the Tonian period, crustal extension allows the deposition of the Embu basin and emplacement of the Juquiá-type granites, that represent a thermal event related to the final stages of the Rodinia break-up, during expansion of one of the possible branches of the Adamastor Ocean. The JG records a transitional tectonic setting, emplaced in a continental extensional deformation environment and/or during intraplate magmatism where partial melting of

upper and even middle-crust occurred. The LA-ICP-MS U—Pb zircon analyses provide significant information about the evolution of the JG since the 800 Ma crystallization.

- Thrusting of AT over ET with maximum age of 660 Ma occurred before the development of the main Ediacaran shear zones.
- The record around 600 Ma is related to pervasive magmatism that took place in the terrane, including emplacement of SBG and possibly to a transpressive collision between the different tectonic blocks.
- The Ediacaran SBG derived from continental crust or underplated crust that has been through a cycle of continent-continent collision shows evidences of a *syn*-tectonic crystallization, i.e., the Sete Barras-type magmatism was formed in a local transtensional area in a regional compressive environment, and the final stages of crystallization may have been influenced by the strain due to surrounding shear zones.
- The record of 578 Ma obtained in metamorphic growth in several zircons of SBG is possibly associated to the final collisional phase in the Ribeira Belt, juxtaposition of the Embu, Coastal (Mongaguá Domain) and Curitiba terranes, when the tectonic escape took place through major NE/SW shear zones.
- The Coastal Terrane is understood as part of the Congo Craton, and its wedge configuration between the Embu and Curitiba terranes is due to the sinistral Itariri shear zone movement.

Acknowledgments

The authors thank FAPESP (Processes 2013/24316-7 and 2015/03737-0) for the financial support to this work and the Geochronological Research Center (CPGeo) of the Geosciences Institute – USP. We are highly grateful to received constructive comments by two reviewers Prof. Vinod Singh and an anonymous reviewer as well as the Editor-in-Chief Michael Roden for his editorial handling.

Appendix A. Supplementary data

Supplementary data to this article can be found online at https://doi.org/10.1016/j.lithos.2019.05.024.

References

Almeida, F.F.M., Brito Neves, B.B., Carneiro, C.D.R., 2000. The origin and evolution of the South American Plataform. Earth Sci. Rev. 50, 77–111.

Alves, A., Janasi, V.A., Campos Neto, M.C., Heaman, L., Simonetti, A., 2013. U–Pb geochronology of the granite magmatism in the Embu Terrane: Implications for the evolution of the Central Ribeira Belt, SE Brazil. Precambrian Res. 230, 1–12.

Alves, A., Janasi, V.A., Campos Neto, M.C., 2016. Sources of granite magmatism in the Embu Terrane (Ribeira Belt, Brazil): Neoproterozoic crust recycling constrained by elemental and isotope (Sr–Nd–Pb) geochemistry. J. South Am. Earth Sci. 68, 205–223.

Babinski, M., Tassinari, C.G.C., Nutman, A.P., Sat, K., Martin, P.R., Iye, S.S., 2001. U/Pb shrimp zircon ages of migmatites from the basement of the Embu Complex Ribeira Fold Belt Brazil: Indications for ~1.4–1.3 Ga Pb–Pb and Rb–Sr "isochron" ages of no geological meaning. South America Symposium on Isotope Geology, 3, Pucón. Book of Abstracts, pp. 91–93.

Basei, M.A.S., Siga, O., Kaulfuss, G.A., Cordeiro, H., Nutman, A., Sato, K., Cury, L.F., Prazeres Filho, H.J., Passarelli, C.R., Harara, O.M., Reis Neto, J.M., Weber, W., 2003. Geochronology and isotope geochemistry of Votuverava and Perau Mesoproterozoic basins, Southern Ribeira Belt, Brazil. South American Symposium on Isotope Geology, 4, Salvador. Short Papers, pp. 501–504.

Basei, M.A.S., Nutmann, A.P., Siga, O., Passarelli, C.R., Drukas, C.O., 2009. The evolution and tectonic Detting of the Luis Alves Microplate of Southeastern Brazil: an exotic terrane during the assembly of Western Gondwana. In: Gaucher, C., Sial, A.N., Halverson, G.P., Frimmel, H.E. (Eds.), Neoproterozoic–Cambrian Tectonics, Global Change and Evolution: A Focus on Southerwestern Gondwana. vol. 16. Elsevier, pp. 273–291.

Basei, M.A.S., Brito Neves, B.B., Siga, O., Babinski, M., Pimentel, M.M., Tassinari, C.C.G., Hollanda, M.H.B., Nutman, A., Cordani, U.G., 2010. Contribution of SHRIMP U Pb zircon geochronology to unravelling the evolution of Brazilian Neoproterozoic fold belts. Precambrian Res. 183, 112–144.

Basei, M.A.S., Frimmel, H.E., Campos Neto, M.C., Araújo, C.E.G., Castro, N.A., Passarelli, C.R., 2018. The Tectonic History of the Southern Adamastor Ocean Based on a Correlation of the Kaoko and Dom Feliciano Belts. Geology of Southwest Gondwana. Regional Geology Reviews, Chap. 3, 63–85.

Ben Othman, D., White, W.M., Patchett, J., 1989. The geochemistry of marine sediments, island arc magma genesis, and crust–mantle recycling. Earth Planet. Sci. Lett. 94, 1–21.

Benetti Silva, B.Y., 2017. Evolução tectônica da porção central do terreno Embu ao norte da Zona de Cisalhamento Taxaquara–Guararema. Master dissertation. Geoscience Institute, p. 121.

Brito Neves, B.B., Campos Neto, M.C., Fuck, R.A., 1999. From Rodinia to Western Gondwana, an approach to the Brasiliano–Pan African Cycle and orogenic collage. Episodes 2, 155–166.

Brito Neves, B.B., Fuck, R.A., Pimentel, M.M., 2014. The Brasiliano collage in South America: a review. Braz. J. Geol. 44, 493–518.

Bruno, H., Almeida, J., Heilbron, M., Salomão, M., Cury, L.F., 2018. Architecture of major Precambrian tectonic boundaries in the northern part of the Dom Feliciano Orogen, southern Brazil: Implications for the West Gondwana amalgamation. J. South Am. Earth Sci. 86, 301–317.

Campanha, G.A.C., Brito Neves, B.B., 2004. Frontal and Oblique Tectonics in the Brazilian Shield. Episodes 27, 255–259.

Campanha, G.A.C., Basei, M.A.S., Tassinari, C.C., Nutman, A.P., Faleiros, F.M., 2008. Constraining the age of the Iporanga formation with SHRIMP U-Pb zircon: implications for possible Ediacaran glaciation in the Ribeira Belt, SE Brazil. Gondw. Res. 13, 117–125.

Campanha, G.A.C., Basei, M.A.S., Faleiros, F.M., Nutman, A.P., 2016. The Mesoproterozoic to early Neoproterozoic passive margin Lajeado Group and Apiaí Gabbro, Southeastern Brazil. Geosci. Front. 7, 683–694.

Campanha, G.A.C., Faleiros, F.M., Cawood, P.A., Cabrita, D.I.G., Ribeiro, B.V., Basei, M.A.S., 2019. The Tonian Embu Complex in the Ribeira Belt (Brazil): revision, depositional age and setting in Rodinia and West Gondwana. Precambrian Res. 320, 31–45.

Campos Neto, M.C., 2000. In: Cordani, U.G., Milani, E.J., Thomas Filho, A., Campos, D.A. (Eds.), Orogenic Systems from Southwestern Gondwana: An Approach to Brasiliano–Pan African Cycle and Orogenic Collage in Southeastern Brazil. Tectonic Evolution of South America, Rio de Janeiro, pp. 335–365.

Campos Neto, M.C., Basei, M.A.S., Vlach, S.R.F., Caby, R., Szabó, G.A.J., Vasconcelos, P., 2004. Migração de orógenos e superposição de orogêneses: Um esboço da colagem brasiliana no sul do Cráton do São Francisco, SE–Brasil. Geol USP 4 (1), 13–40.

Cordani, U.G., Coutinho, J.M.V., Nutman, A.P., 2002. Geochronological constraints on the evolution of the Embu Complex, Sao Paulo, Brazil. J. South Am. Earth Sci. 14, 903–910.

Corfu, F., Hanchar, J.M., Hoskin, P.W.O., Kinny, P., 2003. Atlas of zircon textures. In: Hanchar, J.M., Hoskin, P.W.O. (Eds.), Zircon. vol. 53, pp. 469–500 Mineralogical Society of America Reviews in Mineralogy & Geochemistry.

Costa, R., Trouw, R.A.J., Mendes, J.C., Geraldes, M., Tavora, A., Nepomuceno, F., Araújo, E.B., 2017. Proterozoic evolution of part of the Embu Complex, eastern São Paulo state, SE Brazil. J. South Am. Earth Sci. 79, 170–188.

Cury, L.F., Siga, O., Harara, O.M., Sato, K., Basei, M.A.S., 2008. Geological and geochronological setting of Paranaguá Domain, Ribeira Belt – Southern Brazil. 33 Internatinal Geological Congress, Oslo, CD–ROM.

Dantas, A.S.L., Gimenez Filho, A., Teixeira, A.L., Nagata, N., Fernandes, L.A., Albuquerque Filho, J.L., Frascá, M.H.B.O., 1987. Evolução geológica e estrutural da faixa costeira nas regiões de Juquiá e Miracatu, Sul do Estado de São Paulo. In: Simpósio Regional de Geologia, 6. Rio Claro. Atas SBG 2, 173–189.

DePaolo, D.J., 1981. A neodymium and strontium isotopic study of the Mesozoic calcalkaline granitic batholiths of the Sierra Nevada and Peninsular Ranges, California. J. Geophys. Res. 86, 10470–10488.

DePaolo, D.J., Linn, A.M., Schubert, G., 1991. The continental age distribution: methods of determining mantle separation ages from Sm–Nd isotopic data and application to the southwestern United States. J. Geophys. Res. 96, 2071–2088.

Duffles, P., Trouw, R.A.J., Mendes, J.C., Gerdes, A., Vinagre, R., 2016. U–Pb age of detrital zircon from the Embu sequence, Ribeira belt, SE Brazil. Precambrian Res. 278, 69–86.

Frost, C.D., Frost, B.R., 2008. A geochemical classification for feldspathic igneous rocks. J. Petrol. 49, 1569–1955.

Frost, B.R., Barnes, C.G., Collins, W.J., Arculus, R.J., Ellis, D.J., Frost, C.D., 2001. A geochemical classification for granitic rocks. J. Petrol. 42, 2033–2048.

Fuck, R.A., Brito Neves, B.B., Schobbenhaus, C., 2008. Rodinia descendants in South America. Precambrian Res. 160, 108–126.

Hawkesworth, C.J., Kemp, A.I.S., 2006. Using hafnium and oxygen isotopes in zircons to unravel the record of crustal evolution. Chem. Geol. 226, 144–162.

Heilbron, M., Machado, N., 2003. Timing of terrane accretion in the Neoproterozoic–Eopaleozoic Ribeira orogen (SE Brazil). Precambrian Res. 125, 87–112.

Heilbron, M., Pedrosa-Soares, A.C., Campos Neto, M.C., Silva, L.C., Trouw, R.A.J., Janasi, V.C., 2004. A Província Mantiqueira. Mantesso–Neto V., Bartorelli A., Carneiro C.D.R., Brito Neves BB (Eds.), O Desvendar de um Continente: a moderna geologia da América do Sul e o Legado da Obra de Fernando Flávio Marques de Almeida. Beca, São Paulo, pp. 203–234.

Heilbron, M., Valeriano, C.M., Tassinari, C.C.G., Almeida, J., Tupinambá, M., Siga, O., Trouw, R., 2008. Correlation of Neoproterozoic terranes between the Ribeira Belt, SE Brazil and its African counterpart: comparative tectonic evolution and open questions. Geol. Soc. Lond. Spec. Publ. 294, 211–237.

Heilbron, M., Tupinambá, M., Valeriano, C.M., Armstrong, R., Siva, L.G.E., Melo, R.S., Simonetti, A., Soares, A.C.P., Machado, N., 2013. The Serra da Bolívia Complex: the Record of a New Neoproterozoic Arc–Related Unit at Ribeira Belt. Precambrian Res. 238, 158–175.

Henrique-Pinto, R., Janasi, V.A., Vasconcellos, A.C.B.C., Sawyer, E.W., Barnes, S.J., Basei, M.A.S., Tassinari, C.C.G., 2014. Zircon provenance in meta-sandstones of the São Roque Domain: Implications for the Proterozoic evolution of the Ribeira Belt, SE Brazil. Precambrian Res. 256, 271–288.

Hoskin, P.W.O., 2000. Patterns of chaos: Fractal statistics and the oscillatory chemistry of zircon. Geochim. Cosmochim. Acta 64, 1905–1923.

Janasi, V.A., Vlach, S.R.F., Campos Neto, M.C., Ulbrich, H.H.G.J., 2009. Associated A type subalkaline and high–K calc–alkaline granites in the Itu Granite Province, Southeastern Brazil: petrological and tectonic significance. Can. Mineral. 47, 1505–1526.

Johansson, A., 2014. From Rodinia to Gondwana with the 'SAMBA' model—a distant view from Baltica towards Amazonia and beyond. Precambrian Res. 244, 226–235.
Juliani, C., Hackspacher, P., Dantas, E.L., Fetter, A.H., 2000. The Mesoproterozoic volcano–sedimentary Serra do Itaberaba group of the Central Ribeira belt, São Paulo State, Brazil: implications for the age of the overlaying São Roque group. Revista Brasileira de Geociências 30, 82–86.
Li, Z.X., Bogdanova, S.V., Collins, A.S., Davidson, A., De Waele, B., Ernst, R.E., Fitzsimons, I.C.W., Fuck, R.A., Gladkochub, D.P., Jacobs, J., Karlstrom, K.E., Lu, S., Natapov, L.M., Pease, V., Pisarevsky, S.A., Thrane, K., Vernikovsky, V., 2008. Assembly, configuration, and break–up history of Rodinia: a synthesis. Precambrian Res. 160, 179–210.
Ludwig, K.R., 2012. User's Manual for Isoplot 3.75: A Geochronological Toolkit for Microsoft Excel. Berkeley Geochronology Center Special Publication 5, p. 75.
Maniar, P.D., Piccoli, P.M., 1989. Tectonic discrimination of granitoids. Geol. Soc. Am. Bull. 101, 635–643.
Maurer, V.C., Alves, A., Campos Neto, M.C., 2015. Characterization of the Rio Capivari complex, basement of the Embu Terrane: Geochemical and Geochronological constraints. 8th Hutton Symposium on Granites and Related Rocks (Book of abstracts, PT.164).
McDonough, W.F., Sun, S.S., 1995. The composition of the Earth. Chem. Geol. 120, 223–253.
Medeiros, S.R., Mendes, J.C., McReath, I., Wiedemann, C.M., 2003. U-Pb and Rb-Sr dating and isotopic signature of the charnockitic rocks from Varzea Alegre intrusive complex, Espírito Santo, Brazil. South American Symposium on Isotope Geology, 4, Salvador, Short Papers. 2003, pp. 609–612.
Meira, V.T., García–Casco, A., Juliani, C., Almeida, R.P., Schorscher, J.H.D., 2015. The role of intracontinental deformation in supercontinent assembly: insights from the Ribeira Belt, Southeastern Brazil (Neoproterozoic West Gondwana). Terra Nova 27, 206–217.
Middlemost, E.A.K., 1985. Magmas and Magmatic Rocks: An Introduction to Igneous Petrology. Longman Group Limited, p. 266.
Miller, J.S., Matzel, J.E.P., Miller, C.F., Burgess, S.D., Miller, R.B., 2007. Zircon growth and recycling during the assembly of large, composite arc plutons. J. Volcanol. Geotherm. Res. 167, 282–299.
Mori, P.E., Reeves, S., Correia, C.T., Haukka, M., 1999. Development of a fused glass disc XRF facility and comparison with the pressed powder pellet technique at Instituto de Geociências, São Paulo University. Revista Brasileira de Geociências 29, 441–446.
Navarro, M.S., Andrade, S., Ulbrich, H., Gomes, C.B., Girardi, V.A.V., 2008. The direct determination of rare earth elements in basaltic and related rocks using ICP–MS: testing the efficiency of microwave oven sample decomposition procedures. Geostandards and Research Geoanalytical 32, 167–180.
Passarelli, C.R., Basei, M.A.S., Campos Neto, M.C., Siga, O., Prazeres Filho, H.J., 2004. Geocronologia e geologia isotópica dos terrenos Pré–Cambrianos da porção sul–oriental do Estado de São Paulo. Geologia USP 4, 55–74.
Passarelli, C.R., Basei, M.A.S., Wemmer, K., Siga, O., Oyhantçabal, P., 2011. Major shear zones of southern Brazil and Uruguay: escape tectonics in the eastern border of Rio de la Plata and Paranapanema cratons during the Western Gondwana amalgamation. Int. J. Earth Sci. 100, 391–414.
Passarelli, C.R., Basei, M.A.S., Siga, O., Cavalcante da Silva, P., Shinoda, R., 2016. New U–Pb LA–ICP–MS ages from granitic and migmatitic rocks of the Costeiro Terrane, Mongaguá Domain, Southeastern Brazil: some petrogenetic implications. South American Symposium on Isotope Geology, 10, Puerto Vallarta, Mexico CD of Abstracts.
Passarelli, C.R., Basei, M.A.S., Siga Jr., O., Harara, O.M.M., 2018. The Luis Alves and Curitiba Terranes: Continental Fragments in the Adamastor Ocean. Geology of Southwest Gondwana, Regional Geology Reviews, pp. 189–215 Chap. 8.
Peccerillo, A., Taylor, S.R., 1976. Geochemistry of Eocene calc–alkaline volcanic rocks from the Kastamonu area, northern Turkey. Contrib. Mineral. Petrol. 58, 63–81.
Pedrosa–Soares, A.C., Vidal, P., Leonardos, O.H., Brito Neves, B.B., 1998. Neoproterozoic Oceanic Remnants in Eastern Brazil: further evidence and Refutation of an Exclusively Ensialic Evolution for the Aracuaí–West Congo Belt. Geology 26, 519–522.
Pedrosa–Soares, A.C., Noce, C.M., Wiedemann, C.M., Pinto, C.P., 2001. The Araçuaí –West–Congo Orogen in Brazil: an overview of a confined orogeny formed during Gondwanaland assembly. Precambrian Res. 110, 307–323.
Pupin, J.P., 1980. Zircon and granite petrology. Contrib. Mineral. Petrol. 73, 207–220.
Sato, K., Siga, O., Silva, J.A., McReath, I., Liu, D., Iizuka, T., Rino, S., Hirata, T., Sproesser, W.M., Basei, M.A.S., 2009. In situ isotopic analyses of U and Pb in Zircon by remotely operated SHRIMP II, and Hf by LA-ICP-MS: an example of dating and genetic evolution of zircon by $^{176}Hf/^{177}Hf$ from the Ita Quarry in the Atuba Complex, SE Brazil. Geol. USP, Série Cientifica São Paulo 9, 61–69.
Sato, K., Basei, M.A.S., Ferreira, C.M., Sproesser, W.M., Vlach, S.R.F., Ivanuch, W., Onoe, A.T., 2011. U–Th–Pb analyses by excimer laser ablation/ICP–MS on MG Brazilian xenotime. Goldschmidt – 2011. Mineral. Mag. 1801.
Schmitt, R.S., Trouw, R.A.J., Medeiros, S.R., Dantas, E.L., 2008. Age and geotectonic setting of Late-Neoproterozoic juvenile mafic gneisses and associated paragneisses from the Ribeira Belt (SE Brazil): geochemistry and Sm-Nd data - implications on Gondwana assembly. Gondw. Res. 13, 502–515.
Siga Jr., O., Basei, M.A.S., Passarelli, C.R., Sato, K., Cury, L.F., McReath, I., 2009. Lower and Upper Neoproterozoic magmatic records in Itaiacoca Belt (Paraná–Brazil): Zircon ages and lithostratigraphy studies. Gondw. Res. 15, 197–208.
Siga Jr., O., Basei, M.A.S., Nutman, A.P., Sato, K., Mcreath, I., Passarelli, C.R., Liu, D., 2011a. Extensional and colisional magmatic records in the Apiaí Terrane, South–Southeastern Brazil: integration of geochronological U–Pb zircon ages. Geologia USP 11, 149–175.
Siga Jr., O., Cury, L.F., Mcreath, I., Ribeiro, L.M.A.L., Sato, K., Basei, M.A.S., Passarelli, C.R., 2011b. Geology and geochronology of the Betara Region in South–Southeastern Brazil: evidence for possible Statherian (1.80–1.75 Ga) and Calymmian (1.50–1.45 Ga) extension events. Gondw. Res. 19, 260–274.
Silva, L.C., McNaughton, N.J., Armstrong, R., Hartmann, L.A., Fletcher, I.R., 2005. The Neoproterozoic Mantiqueira Province and its African connections: a zircon–based U–Pb geochronologic subdivision for the Brasiliano/Pan–African systems of orogens. Precambrian Res. 136, 203–240.
Siqueira, R., Hollanda, M.H.B.M., Basei, M.A.S., 2014. A novel approach to (LA–ICP–MS acquired) U–Th–Pb data processing. IX South–American Symposium on Isotope Geology. Chile, 2014, p. 306 Program and Abstracts.
Taylor, S.R., McLennan, S.M., 1985. The Continental Crust: Its Composition and Evolution. Blackwell Scientific Publication, Carlton, p. 312.
Trouw, R.A.J., Peternel, R., Ribeiro, A., Heilbron, M., Vinagre, R., Duffles, P., Trouw, C.C., Fontainha, M., Kussama, H.H., 2013. A new interpretation for the interference zone between the southern Brasília belt and the Central Ribeira belt, SE Brazil. J. South Am. Earth Sci. 48, 43–57.
Tupinambá, M., Heilbron, M., Valeriano, C.M., Porto, R., Dios, F.B., Machado, N., Silva, L.G.E., Almeida, J.C.H., 2012. Juvenile contribution of the Neoproterozoic Rio Negro Magmatic Arc (Ribeira Belt, Brazil): Implications for Western Gondwana amalgamation. Gondw. Res. 21, 422–438.
Vlach, S.R.F., 2001. Micropobe Monazite Constraints for an early (ca. 790 Ma) Brasiliano Orogeny: the Embu Terrane, Southeastern Brazil. III South–American Symposium on Isotope Geology. Chile, 2001 Extended Abstracts.
White, W.M., 2015. Isotope Geochemistry. 1st edition. John Wiley and Sons Ltd, Oxford, p. 496 (ISBN: 978-0-470-65670-9).
Zindler, A.W., Hart, S.R., 1986. Chemical geodynamics. Annu. Rev. Earth Planet. Sci. 14, 493–571.